Hafnium isotope systematics of zircon in high-grade metamorphic rocks of the Anabar shield, Siberia: Radiogenic Hf without mantle input?

Hugo Moreira, Bruno Dhuime, Dmitri Ionov, Anda Buzenchi, Nicolay Gusev

Chemical Geology 636 (2023) 121644

Contents lists available at ScienceDirect

Chemical Geology

journal homepage: www.elsevier.com/locate/chemgeo

Hafnium isotope systematics of zircon in high-grade metamorphic rocks of the Anabar shield, Siberia: Radiogenic Hf without mantle input?

Hugo Moreira [a,*], Bruno Dhuime [a], Dmitri Ionov [a], Anda Buzenchi [a], Nicolay Gusev [b]

[a] Géosciences Montpellier, CNRS & Université de Montpellier, France
[b] Karpinsky Russian Geological Research Institute, 199106 St. Petersburg, Russian Federation

ARTICLE INFO

Editor: Marco Fiorentini

Keywords:
Plate tectonics
Siberian craton
High-grade metamorphism
Zircon
Hf isotopes

ABSTRACT

The timing for the onset of plate tectonics, along with the secular changes in the tectonic settings of continental crust formation, continue to be debated. Recent interpretations based on the increase in zircon $^{176}Hf/^{177}Hf$ ratios at the time of crystallisation (expressed as $\varepsilon Hf_{(t)}$ with respect to chondritic evolution) have been used to ascertain changes in geodynamic settings in the early Earth, specifically in the 3.8–3.6 Ga interval. This increase is widely interpreted as a change in magma generation, from source(s) dominated by ancient crust to source(s) dominated by juvenile inputs from the mantle. At issue, Hf isotope variations remain limited in the early Earth due to the long decay of the Lu—Hf system. This feature, along with the scarcity of rocks and minerals of Eo/Mesoarchaean and Hadean ages, generate large uncertainties over the nature and the timing of the interactions between mantle and crustal reservoirs. The distinction between mantle and crustal sources becomes much clearer in the Palaeoproterozoic, and the study of ancient terranes with several billion years of protracted crustal evolution may hold the key to unlock complex mantle–crust interactions. Here we investigate high-grade metamorphic rocks from the Anabar shield, which contain zircons that crystallised between the Eoarchaean (oldest core at 3814 ± 16 Ma) and the Palaeoproterozoic (youngest core at 2251 ± 15 Ma and youngest rim at 1910 ± 21 Ma). The combination of in situ U—Pb and Hf isotope analyses in zircon indicates the formation of the continental crust in the Siberian Craton in the Eoarchaean, and a conspicuous metamorphic event at 2.0–1.9 Ga. We demonstrate that 2.0–1.9 Ga zircon ages reflect recrystallisation processes under subsolidus conditions, involving the breakdown of high-Lu/Hf minerals (i.e. garnet and pyroxene). The $\varepsilon Hf_{(t)}$ shift at 2.0–1.9 Ga towards more radiogenic values may not be related to a change in magmatic style and sources, but rather to resetting of the Lu—Hf system in response to heating and metamorphic reactions on a mineral scale. Our findings challenge the widely-evoked mechanism of changes in tectonic style and magma sources to account for vertical arrays in the $\varepsilon Hf_{(t)}$ versus crystallisation age space. This calls for considering alternative options, including those based on petrographic data, when interpreting Hf isotope variations in the Hadean/Archaean detrital zircon record.

1. Introduction

U—Pb and Lu—Hf isotope analyses in zircon have been widely used to understand the formation and the evolution of the Earth's continental crust (e.g., Hawkesworth and Kemp, 2006; Iizuka et al., 2009; Belousova et al., 2010; Dhuime et al., 2012; Guitreau and Blichert-Toft, 2014; Roberts and Spencer, 2015; Vervoort and Kemp, 2016; Puetz and Condie, 2019; Bauer et al., 2020a, 2020b; Whitehouse et al., 2022). Recently, there has been increasing interest in identifying what are commonly referred to as 'vertical shifts' in $\varepsilon Hf_{(t)}$ versus crystallisation age diagrams (Fig. 1, red arrows). These vertical shifts reflect an important variation in the $^{176}Hf/^{177}Hf$ ratios relative to the chondritic reservoir at a given time (expressed as $\varepsilon Hf_{(t)}$). The shifts to higher $\varepsilon Hf_{(t)}$ values are widely interpreted as a change in the composition of magma sources from crust-dominated (i.e. reworking) to mantle-dominated (i.e. additions from primitive or depleted mantle reservoirs) (Fig. 2a). This shift was attributed to a change in the tectonic setting of continental crust formation, from stagnant lid to mobile lid tectonics (Næraa et al., 2012; Bauer et al., 2020a). Depending on the zircon databases used, the transition from stagnant to mobile lid tectonics may have occurred at 3.2–3.0 Ga (Næraa et al., 2012; Kirkland et al., 2021), or even earlier at 3.8–3.6 Ga (Bauer et al., 2020a, 2020b; Ranjan et al., 2020; Mulder

* Corresponding author.
E-mail address: hugo.moreira@umontpellier.fr (H. Moreira).

https://doi.org/10.1016/j.chemgeo.2023.121644
Received 17 March 2023; Received in revised form 21 June 2023; Accepted 29 July 2023
Available online 31 July 2023

et al., 2021; dos Santos et al., 2022; Drabon et al., 2022).

An alternative interpretation for the important scatter of $\varepsilon Hf_{(t)}$ values at specific times is the dissolution and recrystallisation of zircons at high-grade metamorphic conditions, along with the breakdown of Lu-rich minerals (Zheng et al., 2004; Kemp et al., 2019; Hammerli and Kemp, 2021). In such a context, metamorphic reactions have a potential to release radiogenic Hf from high-Lu/Hf minerals (Smith et al., 1987) to be later incorporated in recrystallising zircons (Zheng et al., 2004; Chen et al., 2010; Kemp et al., 2019). This process may ultimately lead to the generation of 'juvenile' Hf isotope signatures that mimic mantle additions (Fig. 2b). Schematic diagrams for the interaction between lithospheric reservoirs capable of producing vertical $\varepsilon Hf_{(t)}$ isotope arrays are presented in Fig. 2, with two possible scenarios depending on whether changes in magmatic or metamorphic conditions are considered.

Mantle–crust interaction processes form geochemical reservoirs with different parent/daughter ratios, and their radiogenic isotope ratios become increasingly different with time (e.g., DePaolo and Wasserburg, 1976; Blichert-Toft and Albarède, 1997), to a point at which their respective isotope compositions can be distinguished with the analytical precision of current techniques (e.g., Fisher et al., 2020; Hammerli and Kemp, 2021; Barrote et al., 2022). Crucially, the identification of mantle–crust interactions in the zircon record depends on i) the timing of events between new crust generation and crustal reworking and/or high-grade metamorphism; and ii) the detection of small isotope variations with the current spatial resolution and analytical precision of LA-MC-ICP-MS techniques. In situ Hf isotope analyses in zircon are rarely more precise than ±0.5 εHf units (e.g., Fisher et al., 2011), and when considering uncertainties for both chondritic and depleted mantle reservoirs (i.e. ± 0.4 εHf units – Chauvel and Blichert-Toft, 2001; Bouvier et al., 2008), mantle–crust interaction events remain difficult to decipher in the first ~1.5 billion years of Earth's evolution, unless the 'least disturbed' zircon data with the highest analytical precision are considered (e.g., Kemp et al., 2010; Fisher and Vervoort, 2018; Buzenchi et al., 2022).

The Anabar shield, a remote area north of the Arctic circle on the Siberian Craton, is a largely underexplored Precambrian complex, which offers an opportunity to better understand early mantle–crust interaction. The continental lithospheric mantle of the craton formed in at least two stages, in the Archaean (>2.5 Ga) and in the Palaeoproterozoic (~1.8 Ga) (e.g., Ionov et al., 2015, 2020). The shield contains a range of lower crustal lithologies that bear evidence for crustal reworking since the Eoarchaean (e.g., Gusev et al., 2020a), and a shift towards higher $\varepsilon Hf_{(t)}$ values at 2.0–1.8 Ga was recently reported in zircons from other sites on the Siberian Craton (Skuzovatov et al., 2022; Shatsky et al., 2022). In-depth investigation of Anabar zircons can thus help clarifying the origin of $\varepsilon Hf_{(t)}$ variations at 2.0–1.8 Ga, and overall, it provides new insights into the evolution of the continental crust in the Archean and during the Archaean–Proterozoic transition.

In this study, we combine petrological description, geochemistry, U—Pb geochronology and Lu—Hf isotope data from a range of lithologies on the Anabar shield that contain igneous, detrital and metamorphic zircons. Our in situ approach makes use of high-precision and high spatial resolution analyses to assess the isotope variability of different compositional domains in single zircon grains. The main goals are i) to establish potential geochemical controls for Hf isotope variability in zircon; ii) to consider alternative scenarios for shifts to higher values in the $\varepsilon Hf_{(t)}$ versus crystallisation age diagrams; and iii) to better understand early Earth processes through changes in Hf isotope composition in both new and recrystallised zircons.

2. Geological context and samples

The Siberian Craton is extensively covered with sediments. It is subdivided, based on geophysical data, into several presumably Archaean tectonic units separated by shear zones that merged and stabilised at 2.1–1.8 Ga (Condie, 1994; Koreshkova et al., 2011; Moyen et al., 2017). Much of what is known about the crust and mantle of the craton has come from studies of xenoliths in kimberlites in its central and northeastern parts. The Anabar shield is the only area of exposed basement in the northern and central craton (Fig. 3). It comprises a variety of deformed granitoids and (± garnet-pyroxene-plagioclase)-gneisses and schists predominantly in the granulite facies, as well as less common quartzite, banded iron formations and marble (Condie, 1994).

Both Archaean and Palaeoproterozoic rocks outcrop on the Anabar shield, but their proportions remain unclear due to scarce geologic and age data (Gusev et al., 2020a). U—Pb dating of detrital zircons from modern sediments (Paquette et al., 2017) and late Proterozoic sedimentary rocks (Priyatkina et al., 2016), as well as of zircon megacrysts in kimberlites near the Anabar shield (Kostrovitsky et al., 2016), mainly yields Palaeoproterozoic ages.

Two main components are identified in tectonic units or 'groups' across the shield: (a) 3.2 to 2.9 Ga deformed tonalite-trondhjemite-granodiorite (TTG) rocks that represent its current upper crust and (b) high-grade metamorphic rocks supposed to represent the lower crust. The latter mainly stem from intense tectonothermal activity at around 2.0–1.8 Ga (Paquette et al., 2017; Gusev et al., 2017; Koreshkova and Downes, 2021), i.e. during the amalgamation of Archaean fragments and the accretion of a Palaeoproterozoic arc to the east of the Anabar shield (Rosen and Turkina, 2007; Gusev et al., 2021). The craton

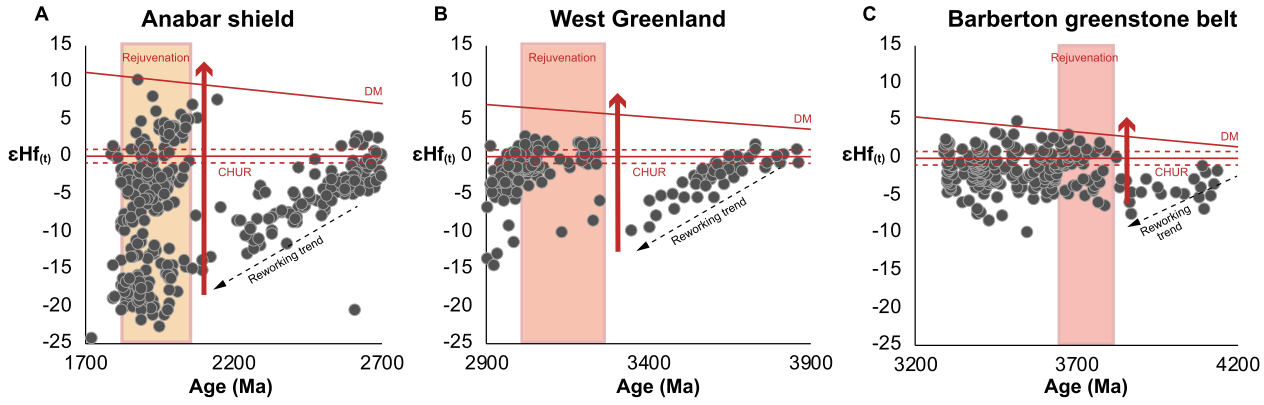

Fig. 1. A) Compilation of zircon Hf isotope data from the Anabar shield, highlighting a significant shift in $\varepsilon Hf_{(t)}$ time-integrated pattern during the Palaeoproterozoic, and commonly interpreted as a main period of continental crust rejuvenation (Skuzovatov et al., 2022 and references therein). B) and C): Comparison with older inferred periods of rejuvenation, in West Greenland (B) (Kirkland et al., 2021), and in South Africa (C) (Drabon et al., 2022). Red arrows point towards more radiogenic (i.e., mantle-like) $^{176}Hf/^{177}Hf$ ratios. (For interpretation of the references to colour in this figure legend, the reader is referred to the web version of this article.)

includes extensive Palaeoproterozoic shear zones that could represent sutures of the Archaean blocks (Fig. 3), although sutures are not clearly constrained in the literature. Finally, a voluminous Palaeoproterozoic magmatism is recorded at the margins of the Siberian Craton and adjacent tectonic zones (Rosen et al., 1994; Donskaya, 2020). A major 2.1–1.8 Ga 'rejuvenation event' of the lower crust across the Siberian craton was suggested from whole-rock Sm—Nd and zircon Lu—Hf isotope analyses (Neymark et al., 1993; Shatsky et al., 2019; Moyen et al., 2017; Paquette et al., 2017; Skuzovatov et al., 2022). Rejuvenation models are based on the observation of a shift towards more radiogenic Nd and Hf isotope compositions, which is particularly evident in zircons from crustal xenoliths in kimberlites (Moyen et al., 2017; Skuzovatov et al., 2022) (Fig. 3a).

Unlike previous studies that examined isotopic variations in the crystalline basement of the Siberian craton using xenoliths in kimberlites, we studied two outcropping localities within the Daldyn group, an exposed segment of Archaean crust reworked in the Palaeoproterozoic (Fig. 3). The Daldyn and Upper Anabar groups are made up of Archaean sequences of gneisses and mafic/ultramafic lenses, intercalated with supracrustal units that reached granulite-facies during the Palaeoproterozoic. The Daldyn group has a higher proportion of mafic lithologies than the Upper Anabar group, (Gusev et al., 2020a). The locality of the six samples selected for this study is shown in Fig. 3b, and their petrological description is presented below.

2.1. Sample 831–2

Sample 831–2 is a garnet-bearing foliated granulite with compositional banding. The bands are cm-thick with alternating felsic and mafic-rich compositions. Felsic bands have few to no mafic minerals and comprise re-crystallised quartz (65%) and plagioclase (35%), with accessory epidote and apatite (1%). Mafic bands consist of re-crystallised quartz (25%), plagioclase (25%), clinopyroxene (15%), titanite (15%), garnet (15%), opaque minerals (5%) and scapolite (<1%). Zircon grains were only identified in the mafic bands. They are ~150 μm long and round, often surrounded by plagioclase. Epidote is only observed in plagioclase alteration products. Some intermediate compositional bands are coarser grained and contain larger crystals of clinopyroxene, biotite and opaques (Fig. 4a). The foliation is better developed in biotite-rich bands, and seems to have formed later than the main high-grade paragenesis. Garnet occurs as coronas separating cpx from plagioclase, i.e. is out of textural equilibrium (Fig. 4b), but equilibrium textures are also observed among cpx-plag-qtz-garnet (Fig. 4c). The granoblastic textures show re-equilibration after most of the deformation took place since the grains are large and relatively equigranular with large inter-grain angles. The sample was divided in three portions based on their abundance of mafic minerals. These portions are called 'mafic', 'intermediate' and 'felsic' in an attempt to examine their compositions separately.

2.2. Sample 607

Sample 607 is a granoblastic mafic granulite composed of plagioclase (30%), clinopyroxene (25%), orthopyroxene (10%), brown hornblende (20%), quartz (10%), opaque minerals (magnetite/ilmenite; 5%), retrogressed biotite and apatite. The mafic granulite contains distinct bands richer in opaques (magnetite up to 50%), which retain granulite facies parageneses with two pyroxenes, magnetite and plagioclase (Fig. 5). Breakdown reactions from pyroxene to amphibole are commonly observed in thin-section (Fig. 5). Some amphiboles appear in equilibrium with clinopyroxene and others show contact reaction, which suggests that this rock re-equilibrated at low granulite to upper amphibolite facies. Epidote is found as alteration phase in plagioclase and clinopyroxene. Ilmenite surrounds amphibole and seems to be in disequilibrium and potentially involved in the breakdown reaction. Zircon grains are round to elongated, euhedral and transparent, and they can reach up to 300 μm.

More felsic portions of the same outcrop (samples 607A and 607B; see Gusev et al. (2020a) were also analysed in this study. Sample 607A has higher proportions of recrystallised quartz (up to 70%). Amphiboles are rare to absent, clinopyroxene and orthopyroxene are roughly in the same proportions (~15%), and opaque minerals represent <10% of the modal composition. Sample 607B consists mostly of coarse-grained plagioclase and quartz (80%) with minor microcline. Almost 20% of the sample is composed of orthopyroxene, up to 1 cm in size. Zircon and apatite are present, along with opaque minerals (5%).

2.3. Sample 177

Sample 177 is a meta-granitoid, geochemically classified as a trondhjemite (Gusev et al., 2017). The foliation is marked by intense alteration of feldspar, vastly replaced by chlorite alongside opaque

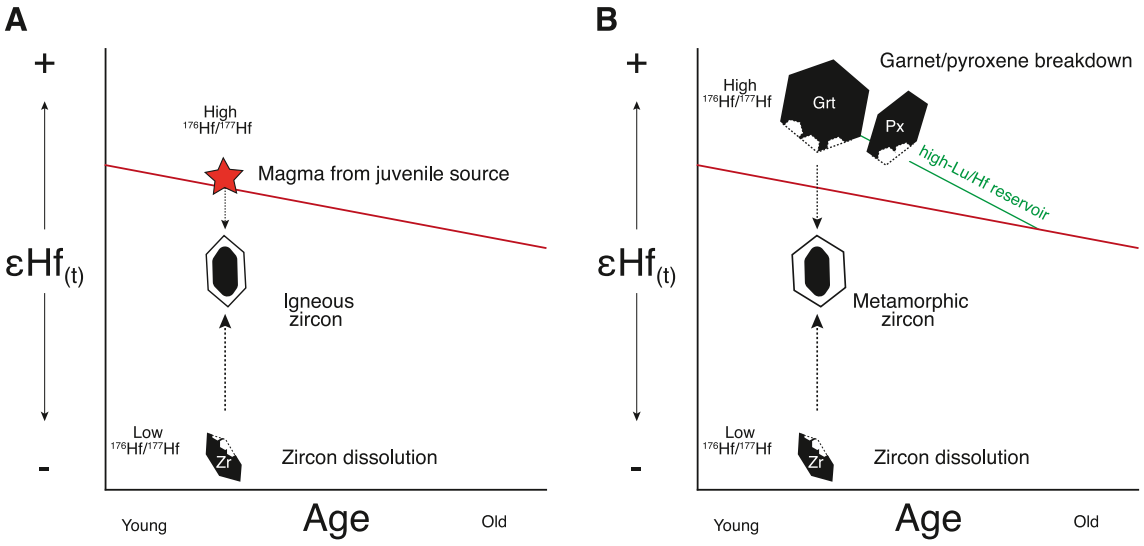

Fig. 2. Schematic representation of $\varepsilon Hf_{(t)}$ variations in zircon as a product of interactions between different isotope reservoirs, in magmatic (A) and metamorphic (B) environments. Both scenarios show a zircon that crystallised from a crustal source that evolved along the dashed orange line after its separation from the mantle, and this zircon recorded the incorporation of radiogenic Hf at time *t* from either A) a mantle-derived magma; or B) the breakdown of a high-Lu/Hf reservoir. Zircons with identical $^{176}Hf/^{177}Hf$ ratios can be produced in both scenarios.

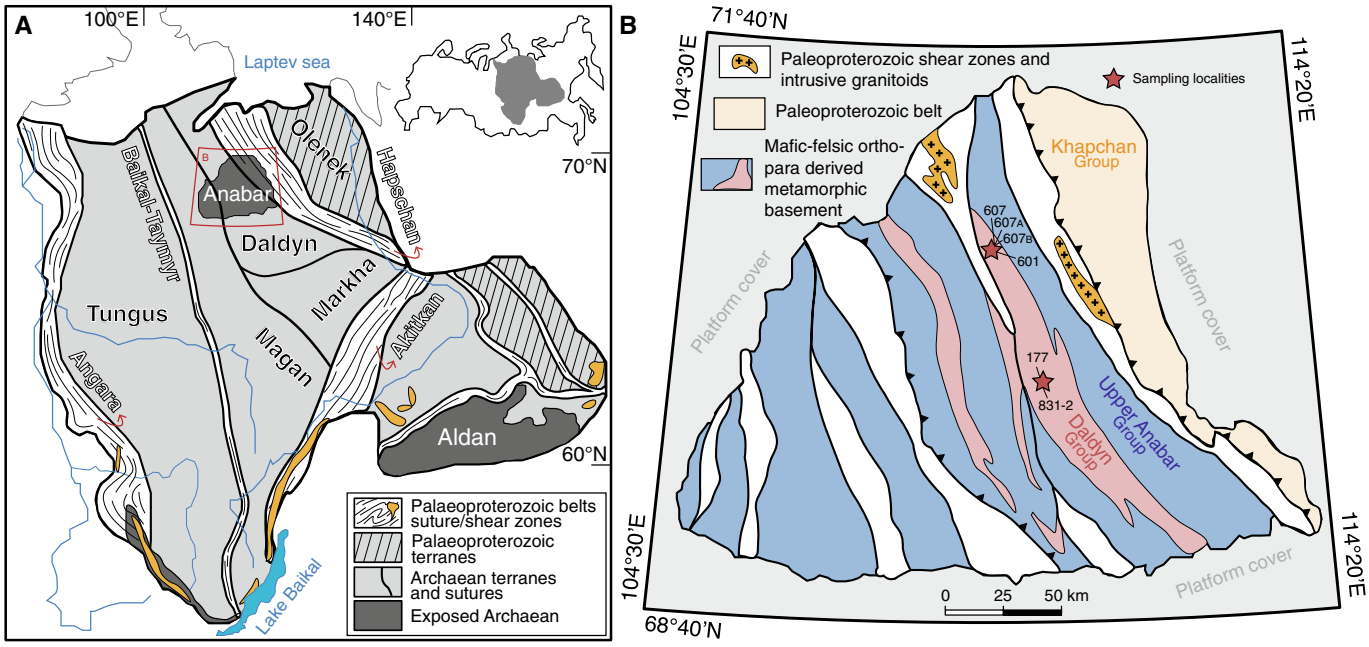

Fig. 3. A) Simplified geological map of the Siberian Craton, in which Archaean terranes and Palaeoproterozoic reworked mobile belts are highlighted. The studied area is delimited by the red field. B) Close view at the studied area (the Anabar Shield) and sample localities. Maps are modified from Paquette et al., 2017; Moyen et al., 2017 and Gusev et al., 2020b. (For interpretation of the references to colour in this figure legend, the reader is referred to the web version of this article.)

minerals (possibly ilmenite). The sample is comprised approximately of 45% feldspar and 45% quartz. Only 1% of this sample is composed of primary biotite and the remaining mafic minerals are magnetite. The foliation is marked by intensive shearing of primary biotite and retrogressed feldspar-rich assemblage (Fig. 6). Large inter-grain angles and dominated felsic composition are suggestive of high-grade metamorphism and compositional segregation during shearing. Petrological, geochemical and isotopic investigation suggest that this sample derives from the partial melting of a more mafic protolith (Gusev et al., 2017). The partial melting and crystallisation of the felsic magma may have occurred at 3292 ± 9 Ma, as indicated by U—Pb dating of the most concordant zircon cores, whereas concordant rims recorded granulite metamorphism at 1926 ± 38 Ma (Gusev et al., 2017).

2.4. Sample 601A

Sample 601A is a proto-mylonite quartzite (Fig. 6), composed of quartz, K-feldspar, garnet, sillimanite and ilmenite. The garnet, feldspar and larger quartz grains are porphyroclasts in augen zones. Recrystallised quartz comprises >80% of the area of the thin-section. All mineral phases record the main deformational event that produced the metamorphic foliation, including garnet and sillimanite. Feldspar (15%) is saussuritized mostly at the edges of the grains, and perthitic texture is common. Plagioclase is also present but rare, and garnet is approximately 5%. Ilmenite and other opaque minerals (magnetite and pyrite) are minor and the few observed zircon grains are both round and elongated (~200 μm). Sillimanite is associated with garnet and seems to be a high-grade assemblage above muscovite+qtz stability as there are no hydrous minerals. Because garnet is involved and stretched along the main mylonitic foliation, it is interpreted that the highest temperature was achieved previously to mylonitization.

3. Methods

Samples were cut and crushed, and aliquots were ground to powder at Karpinskyii Institute (VSEGEI, St Petersburg). Sample powders previously prepared at VSEGEI and additional uncrushed rock aliquots were analysed for major and trace element by XRF and ICP-MS at the SARM (Service d'Analyse des Roches et Minéraux, Nancy), following the approach described in Carignan et al. (2001).

Zircon cathodoluminescence (CL) and back-scattered (BSE) images were acquired at the University of Montpellier, using a FEI Quanta 200 FEG Scanning Electron Microscope (SEM) coupled with a DEBEN Centaurus 400 nm–1200 nm photomultiplier detector. An Oxford Instrument silicon drift Ultim-Max 100 mm^2 detector for Energy Dispersive X-ray Spectroscopy (EDS) analyses was used to confirm petrographic descriptions and identify some opaque phases.

U—Pb and Lu—Hf isotope analyses in zircon were performed by LA-MC-ICP-MS at the MILESTONE Laboratory (RéGEF ISOTOP-MTP, Géosciences Montpellier, France). The lab hosts a Thermo Scientific Neptune XT multicollector inductively-coupled plasma mass spectrometer (MC-ICP-MS) equipped with a multiple ion counters package designed for U—Pb analyses, as well as a Teledyne Cetac Analyte Excite+193 nm ArF excimer laser. The laser has an optional X-Y Theta dynamic aperture that allows rectangular-shaped beams to be delivered.

U—Pb analyses were performed at 12 × 12 μm square beam size, with a laser fluence of 2.0 $J.cm^{-2}$ and a repetition rate of 4 Hz. The He flow in the double-volume cell was set at 450 mL/min and 380 mL/min for the cell and the cup, respectively. The sample gas (Ar) flow was 1 L/min, and a small amount of N_2 (~0.7 mL/min) was added to the mixture before it reached the torch. For each analysis, the gas background was measured for 15 s, followed by 26 s of ablation (400 cycles of 0.066 s). The following masses were measured on the respective detectors: ^{202}Hg (IC4), ^{204}(Pb + Hg)(IC5), ^{206}Pb(L5), ^{207}Pb(IC1), ^{232}Th(H2) and ^{238}U (H4). Each analysis was followed by 10 s of washout. The 91,500 zircon reference material (ID-TIMS age of 1065 ± 1 Ma; Wiedenbeck et al., 1995) was used as primary standard, and Plešovice zircon (ID-TIMS age of 337.1 ± 0.3 Ma; Sláma et al., 2008) and Kaap Valley tonalite zircon (SHRIMP age of 3226 ± 14 Ma; e.g., Armstrong et al., 1990) were used as secondary standard to assess both the precision and accuracy of the measurements. Standards analyses are within 1% of published values (see Supplementary material). Zircon data were processed, corrected for down-hole fractionation and instrumental drift using the Iolite 4 software (Paton et al., 2011; Petrus and Kamber, 2012). This software allows careful examination of time-resolved analyses, which helps identifying analyses performed over different growth domains as well as

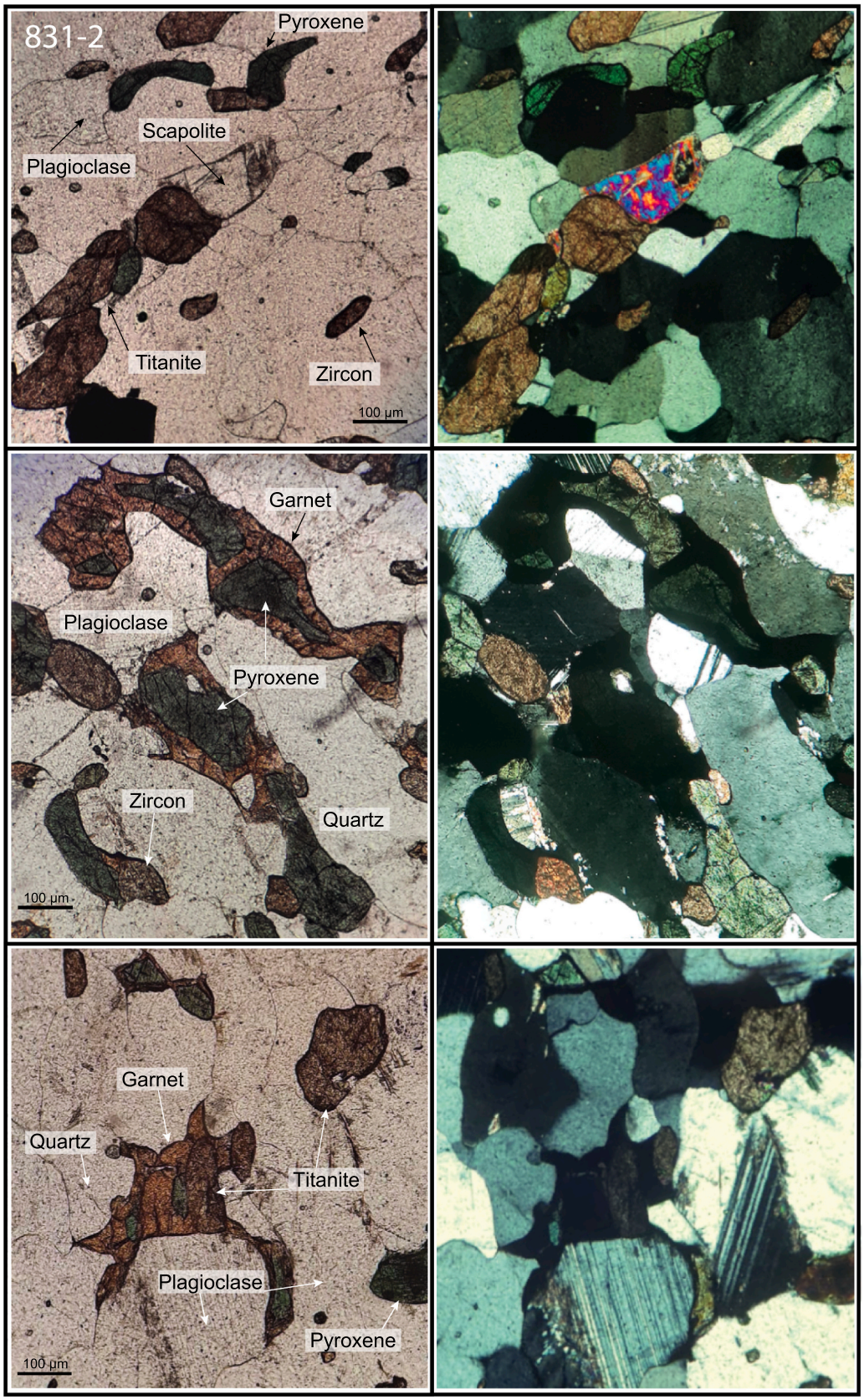

Fig. 4. Thin-section photographs of sample 831–2 in PPL and XPL light showing granoblastic texture. The granulite contains scapolite (A), which suggests high-temperature equilibration, and some pyroxene crystals are surrounded by garnet (B). The lower panel shows garnet in equilibrium with titanite (C).

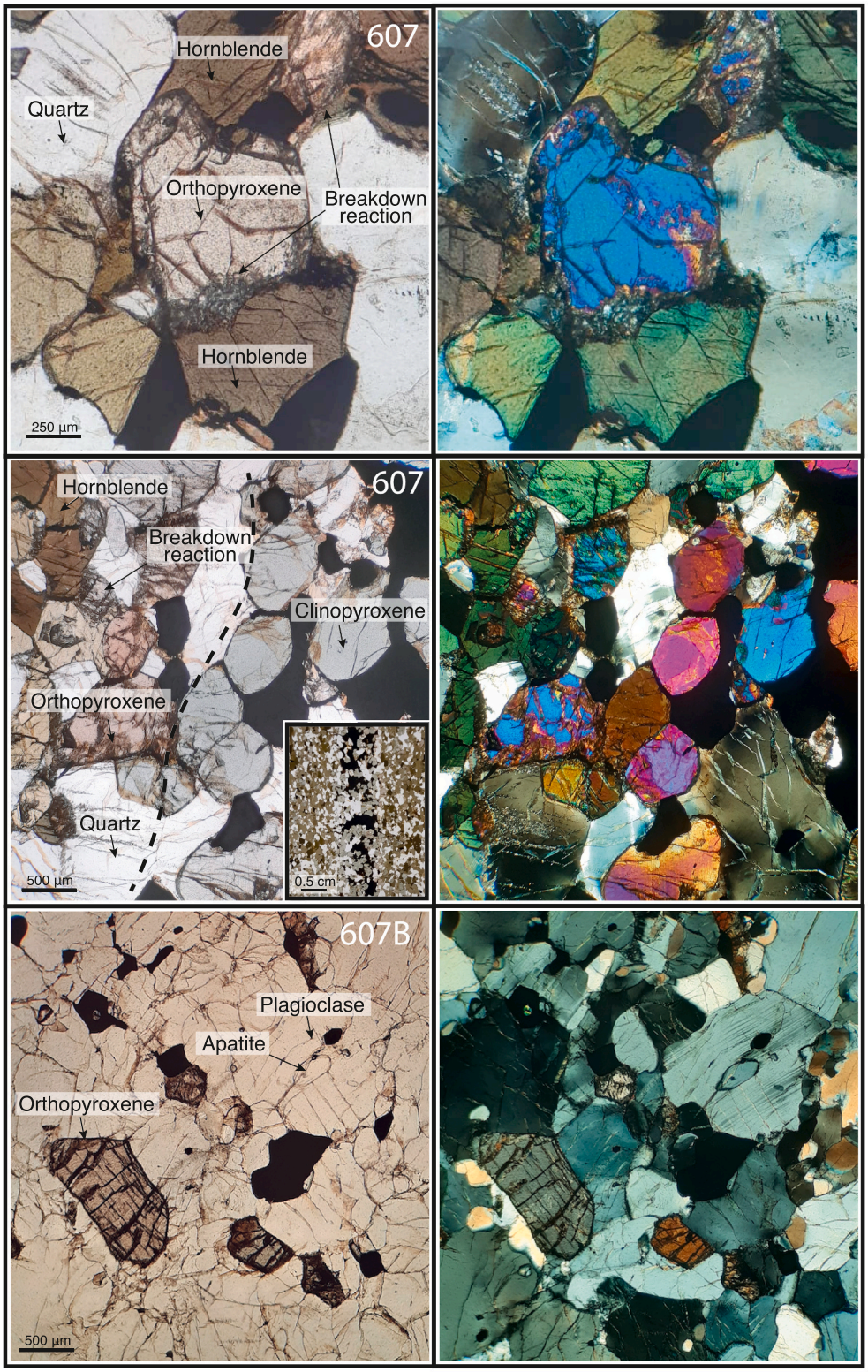

Fig. 5. Thin-section photographs of samples 607 and 607B in PPL and XPL light. Upper panel shows orthopyroxene breakdown reaction to amphibole. Inset in middle left panel shows a larger view of the thin-section with hornblende-free band in the central portion, which retained granulite facies metamorphism. The dashed line roughly marks the contact between them.

potential inclusions. Time-resolved signals with abrupt changes caused either by inclusions and/or ablation of two domains were observed in only 3 out of 400 analyses.

Lu—Hf analyses were performed at square beam sizes of 25 × 25 μm or 40 × 40 μm, depending on the size and homogeneity of the internal structures observed in the zircons. Analyses were done on top of U—Pb spots that yielded concordant (i.e. >90% concordance) ages, and the position of laser beam was carefully adjusted to ensure that only one growth domain were ablated. Nine out of 186 analyses were carried out in zircon rims not previously analysed for U—Pb. Their age was

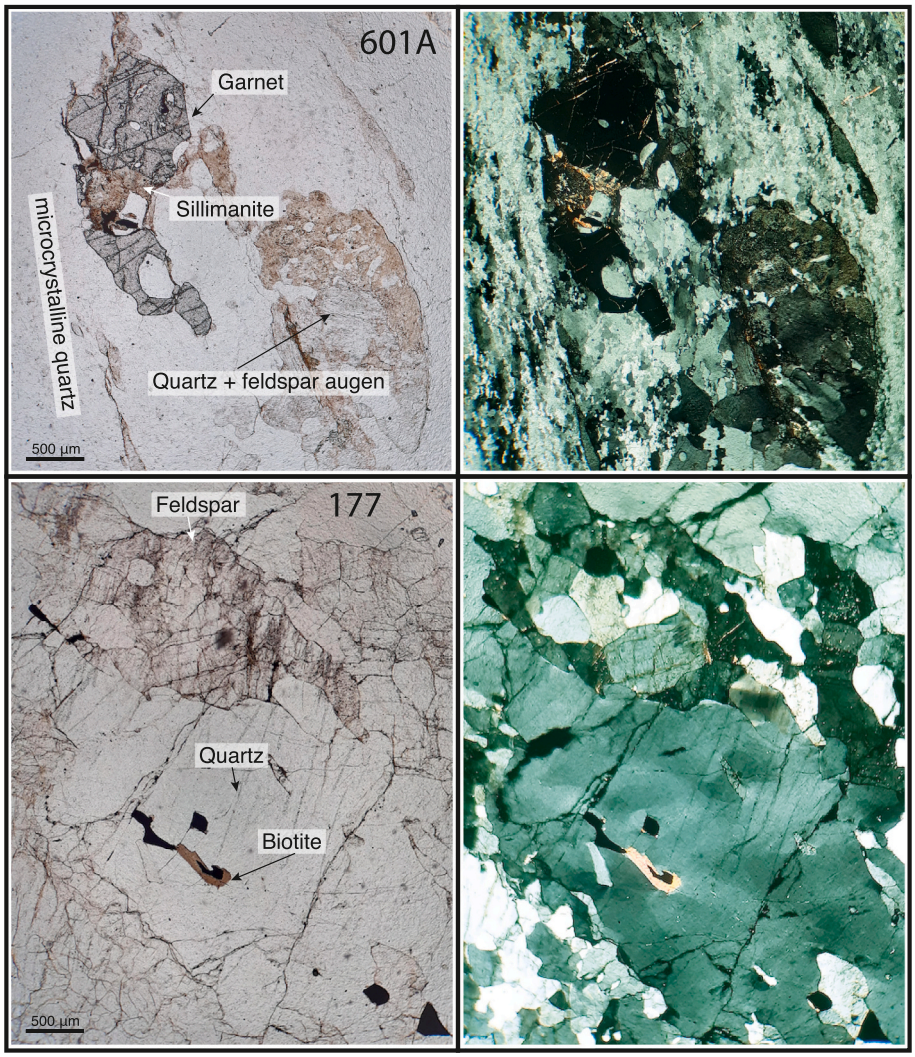

Fig. 6. Thin-section photomicrographs (left, PPL and right, XPL) of samples 601A and 177. Note that garnet is involved in the main foliation of sample 601A.

estimated based on dated zircon rims from the same samples, assuming that all rims represent the same zircon growth episode. A laser fluence of 5.5 J.cm^{-2} and a repetition rate of 5 Hz were used. The He flow was 600 mL/min (cell) and 200 mL/min (cup), and Ar and N_2 flows were the same as for U—Pb analyses. The following masses were measured on Faraday cups connected to 10^{11} Ω amplifiers: 171 (L4), 172 (L3), 173 (L2), 175 (L1), 176 (Axial), 177 (H1), 178 (H2), and 179 (H3). Tuning was done during ablation of NIST 612 glass and Mud Tank zircon, along a ca. 1 mm raster, using a 40 × 40 μm spot, a laser fluence of 5.5 Jcm^{-2} and a repetition rate of 4 Hz. The ^{178}Hf intensity was typically higher than 6.5 V for Mud Tank and higher than 0.03 V for NIST 612. ^{171}Yb, ^{173}Yb and ^{175}Lu were used to correct isobaric interferences of ^{176}Lu and ^{176}Yb on ^{176}Hf, following a method set up at the Bristol Isotope Group and detailed in Fisher et al. (2011). For Yb, the interference-free ^{171}Yb was corrected for mass bias effects using an exponential law and ^{173}Yb/^{171}Yb = 1.132685 (Chu et al., 2002). The mass bias-corrected ^{171}Yb was monitored during the run and the magnitude of the ^{176}Yb interference on ^{176}Hf was calculated using ^{176}Yb/^{171}Yb = 0.901864 (Chu et al., 2002). For Lu, the interference-free ^{175}Lu was corrected for mass bias effects assuming βLu = βYb and using an exponential law. The mass bias-corrected ^{176}Lu was monitored during the run and the magnitude of the ^{176}Lu interference on ^{176}Hf was calculated using ^{176}Lu/^{175}Lu = 0.02655 (Vervoort et al., 2004). Interference-corrected ^{176}Hf/^{177}Hf were corrected for mass bias using an exponential law and ^{179}Hf/^{177}Hf = 0.7325 (Patchett and Tatsumoto, 1981). Finally, a correction of +70 ppm was applied to the final ^{176}Hf/^{177}Hf ratios, to account for a systematic deviation observed between the accepted JMC-475 solution value (0.282160) and that measured on our instrument (see also a discussion in Kemp et al., 2019, based on observations of the Mud Tank zircon). The accuracy and precision of Lu—Hf measurements was monitored via repeated measurements of zircon reference materials. The Plešovice (0.282482 ± 13; Sláma et al., 2008), Mud Tank (0.282507 ± 6; Woodhead and Hergt, 2005) and Temora-2 (0.282686 ± 8; Woodhead and Hergt, 2005) zircons were measured during the session. At 40 × 40 μm beam size, the long-term average ^{176}Hf/^{177}Hf is 0.281484 ± 13 for Plešovice (n = 24; 2 s.d.), 0.282509 ± 15 for Mud Tank (n = 30), and 0.282692 ± 23 for Temora-2 (n = 18). At 25 × 25 μm beam size, the long-term average ^{176}Hf/^{177}Hf is 0.282482 ± 22 for Plešovice (n = 99), 0.282510 ± 28 for Mud Tank (n = 75), and 0.282691 ± 38 for Temora-2 (n = 35). These results are in good agreement with reference values.

4. Results

4.1. Geochemistry

The rocks in this study can be subdivided into metasedimentary and metaigneous based on their mineral assemblages presented in Section 2.

4.1.1. Metasedimentary rocks

The three portions of sample 831–2 have SiO_2 content of 60, 85 and 93 wt% for mafic, intermediate and felsic compositions, respectively. Overall, all portions are low in alkalis. Despite a 20 wt% difference in SiO_2, the two less Si-rich portions have very similar REE patterns. These contrast with the REE pattern of the most felsic portion, which has low REE, a positive Eu anomaly (calculated as $Eu_N/(Sm_N{*}Gd_N)^{1/2}$, where N denotes normalised to average chondrite) and a concave HREE pattern (Fig. 7).

Sample 601A is markedly enriched in Cr (>200 ppm), which indicates that some opaque minerals observed in thin-section may be chromite. REE are depleted and show a similar pattern to that of the most felsic portion of sample 831–2, although with a less pronounced Eu anomaly (Fig. 7). The overall concave HREE pattern is characteristic of samples lacking mafic minerals that incorporate middle REE, such as amphiboles.

4.1.2. Metaigneous rocks

Samples from locality 607 vary in SiO_2 from 44 wt% to 70 wt%. Samples with higher SiO_2 also have higher K_2O, up to 1.6 wt%. The sample with the lowest SiO_2 (607) has the highest total abundance of REE and a negative Eu anomaly, whereas samples with higher SiO_2 (57 and 70 wt%; 607A and 607B, respectively) have relatively lower concentration in REE and no Eu anomaly (Fig. 7). These samples are compositionally similar to garnet-free lower crustal granulites from the same craton (e.g., Moyen et al., 2017).

Sample 177 has 73 wt% SiO_2, high K_2O (>4.4 wt%), a positive Eu anomaly and a steep REE pattern with elevated LREE and depleted REE. This REE pattern is typical of TTGs (Moyen and Martin, 2012) and it contrasts greatly with other samples studied (Fig. 7). However, the sample is more enriched in K_2O ($K_2O/N_2O > 1.2$) and Ba (>1500 ppm) when compared to *stricto* sensu TTG compositions, and has overall low contents of mantle-forming elements (Cr, Ni and Mg). The geochemical characteristics and the absence of amphibole in this sample make it similar to the high-K biotite-granitoids of Moyen (2020), i.e., C-type granitoids. In the ternary diagram for the distinction of Archaean granitoids (Laurent et al., 2014), this sample plots in the field of biotite/two-mica granites.

4.2. Zircon analyses

CL images reveal the presence of core-rim structures in all samples, as well as textural evidence for dissolution and subsequent growth of rim domains. Zircons can be short or elongated, but they distinctively show round terminations (upper panels of Figs. 8a, b, c, d, e, f). Their internal structures vary from largely predominant cores surrounded by 1–10 μm rims, to subordinate cores surrounded by large >50 μm homogenous rims. The rims show generally brighter cathodoluminescence than the cores (Fig. 8a, b, c), but in sample 607 the rims are darker than the cores (Fig. 8e). Some rims range from 50 to 100 μm in thickness and rarely contain inclusions. The inherited cores have feldspar and/or apatite inclusions in roughly 15–25% of the grains. The overall rounded shape of the grains, with rim overgrowths truncating fine oscillatory domains in the cores, is typical of metamorphic zircons that grew at solid-state (e.g., Schaltegger et al., 1999; Hoskin and Black, 2000).

Magmatic cores have U—Pb ages ranging from ca. 2.2 to 3.5 Ga, whereas rims have clearly younger ages between ca. 2.1 and 1.9 Ga. A cluster of concordant to slightly discordant analyses around 1.9 Ga show relatively high (>0.2) Th/U ratios (lower panels of Fig. 8a, b, c, d, e, f), although with no obvious evidence of a magmatic origin from their internal texture. All samples show a discordant scattered array between >3.0 Ga and ~ 1.9–2.1 Ga, with variable Th/U ratios. Some round to elongate grains show no CL or age distinction from core to rim and yield ages between 2.1 and 1.9 Ga (e.g., Fig. 8b, d, e). A small number of analyses that plot close to the Concordia between 2.75 and 2.20 Ga do not fall on the main discordant array; a feature that is observed in sample 831–2 (Fig. 8a). One zircon from sample 607 has three distinct domains, with a 3.8 Ga core surrounded by a 2.5 Ga mantle and a 2.0 Ga rim (Fig. 8e).

Initial $^{176}Hf/^{177}Hf$ ratios were calculated using the apparent

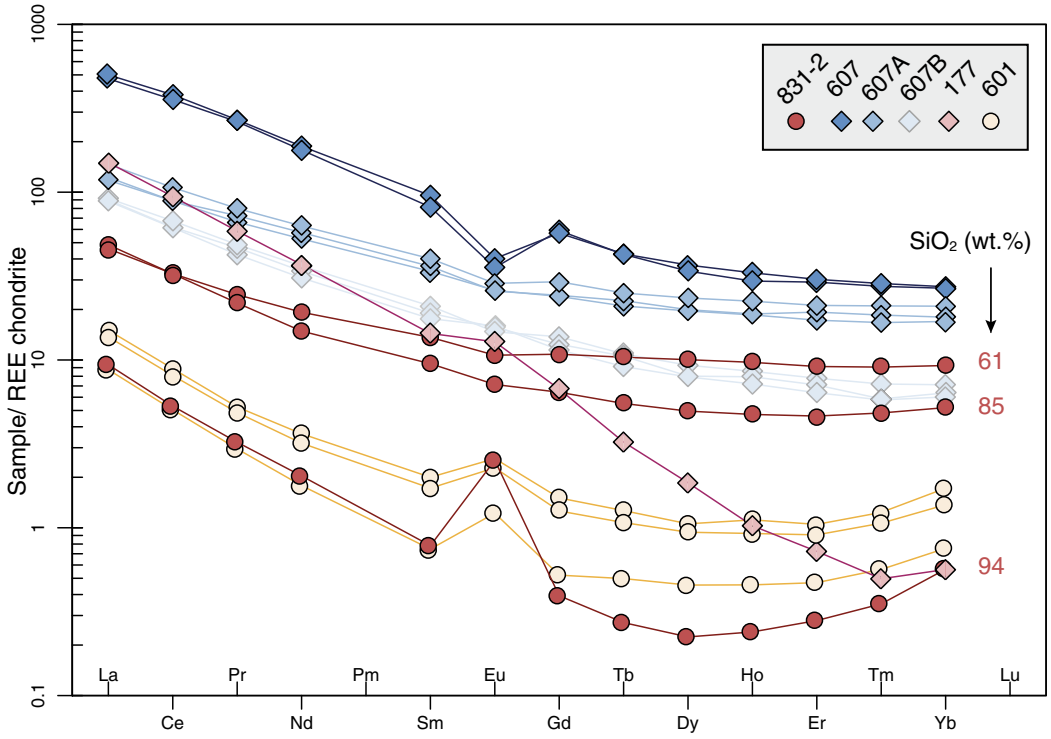

Fig. 7. Chondrite-normalised (Boynton, 1984) REE patterns of whole-rock samples. The SiO_2 (wt%) contents for the three portions of sample 831–2 are indicated on the right-hand side of the REE patterns.

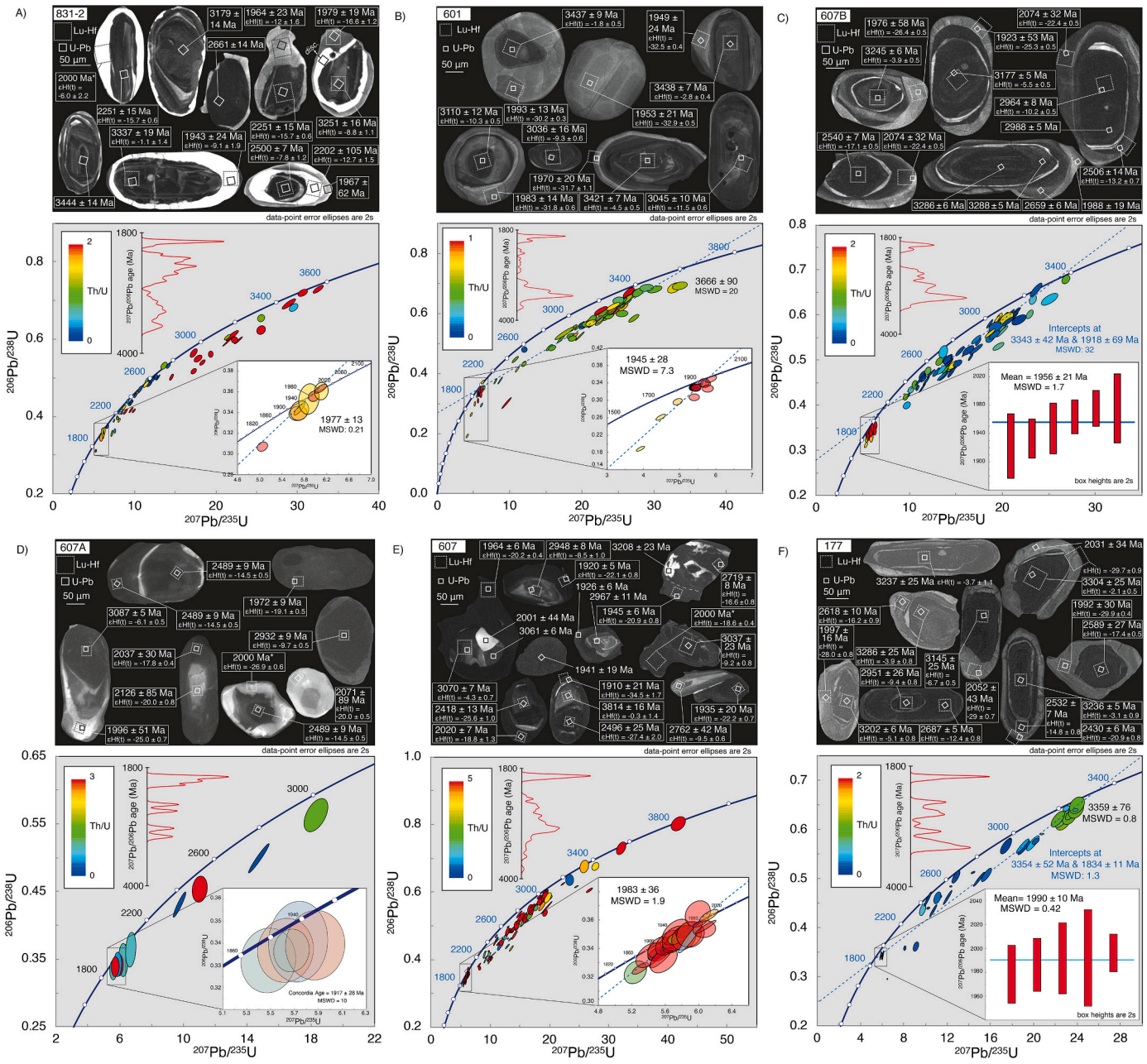

Fig. 8. Zircon CL images and Concordia diagrams for Anabar samples: A) 831–2; B) 177; C) 601A; D) 607A; E) 607B and F) 607. Squares in CL images indicate the location of in situ U—Pb and Lu—Hf analyses performed by LA-MC-ICP-MS. Error ellipses in the Concordia plot are at 2-sigma level and fully propagated. Variations in Th/U ratios (indicated by changes in the colour of the ellipses) point towards unusually high Th/U ratios in zircon rims. The $^{207}Pb/^{206}Pb$ ages are overall bimodal for all samples indicating a young peak at around 1.9 Ga and an older peak at >3.0 Ga.

$^{207}Pb/^{206}Pb$ ages obtained in the same zircon growth domains. Zircon cores have $^{207}Pb/^{206}Pb$ ages ranging between 3.8 and 2.2 Ga, and for each sample a predominant group of core analyses with a broad range of $^{207}Pb/^{206}Pb$ ages but restricted $^{176}Hf/^{177}Hf_{(t)}$ variations (within ±0.0001 units) can be identified. This is illustrated by the horizontal 'Pb-loss' yellow trends in the $^{207}Pb/^{206}Pb$ age versus $^{176}Hf/^{177}Hf_{(t)}$ diagram (Fig. 9a). In contrast, zircon rims yield more restricted $^{207}Pb/^{206}Pb$ ages, between 2.0 and 1.9 Ga. In Fig. 9a, zircon rims from samples 601 and 177 plot on the same horizontal Pb-loss trends as the cores analyses, whereas zircon rims in samples from locality 607 and sample 831–2 have $^{176}Hf/^{177}Hf_{(t)}$ ratios that are up to 0.0006 higher than the $^{176}Hf/^{177}Hf_{(t)}$ ratios of the cores at 2.0–1.9 Ga. This is illustrated by the vertical red arrow in Fig. 9a. In the $\varepsilon Hf_{(t)}$ versus $^{207}Pb/^{206}Pb$ age space, cores and rims analyses of samples 601 and 177 plot along a line with a $^{176}Lu/^{177}Hf = 0$ slope (Fig. 9b). Zircon cores analyses in samples from locality 607 and sample 831–2 also plot along a line with a $^{176}Lu/^{177}Hf = 0$ slope, whereas 2.0–1.9 Ga rims in these samples define a clear vertical shift from $\varepsilon Hf_{(t)} = -35$ to $\varepsilon Hf_{(t)} = -5$. The core-rim pair analyses thus indicate that zircons from samples 601 and 177 follow a $^{176}Lu/^{177}Hf = 0$ slope, whereas the core-rim pairs from samples 607 and 831–2 follow $^{176}Lu/^{177}Hf$ slopes that are different from zero (Fig. 9b). These non-zero slopes are also variable within core-rim pairs of samples 607 and 831–2, with highest $^{176}Lu/^{177}Hf = 0.07$ and lowest $^{176}Lu/^{177}Hf = 0.007$. In summary, Hf isotope variations between zircon cores and rims can be fairly different depending on the mineralogy of the host rocks, and the origin of these variations is further investigated in the sections below.

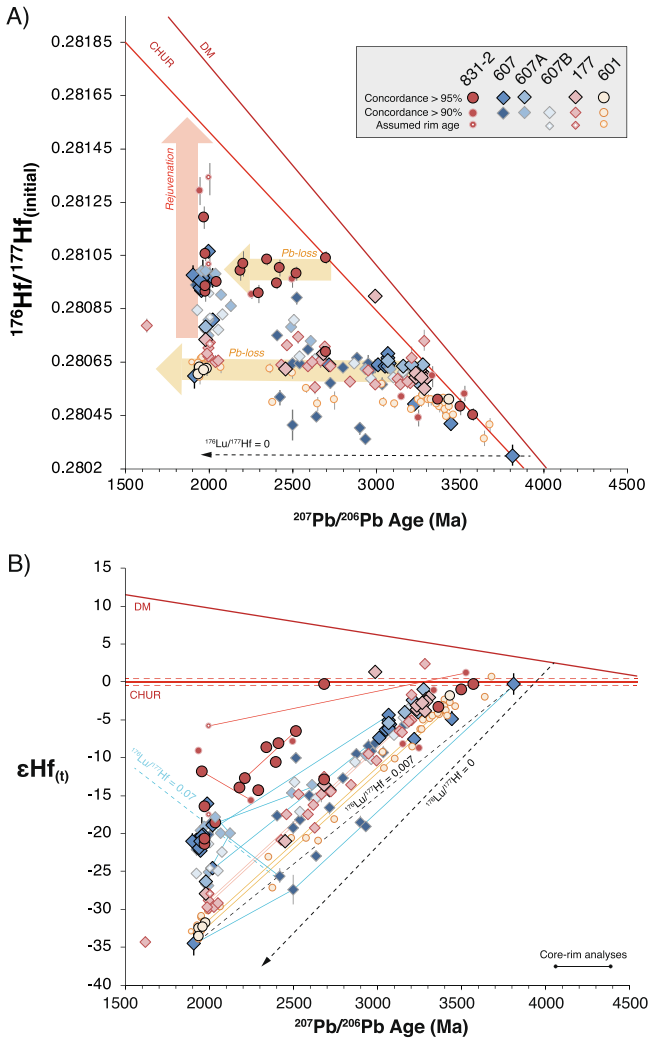

Fig. 9. Zircon Lu—Hf analyses versus crystallisation ages from studied samples. All assigned ages are measured $^{207}Pb/^{206}Pb$ ages. A) Zircon crystallisation age versus initial $^{176}Hf/^{177}Hf$ isotope composition. B) Zircon crystallisation age vs $\varepsilon Hf_{(t)}$ values. Analyses show isotopic variations at around 1.9 Ga that could not be formed by Pb-loss or evolution of an evolved reservoir. Zircon cores and rims reflect radiogenic enrichment that form a vertical array. This vertical array cannot be interpreted as a main period of continental crust rejuvenation because zircon grains are metamorphic and grew in the absence of melt. DM and CHUR evolution lines are after Chauvel and Blichert-Toft (2001) and Bouvier et al. (2008), respectively.

5. Discussion

5.1. Nature of protoliths and age of metamorphism

5.1.1. Metasedimentary rocks

In sample 831–2, garnet, titanite and pyroxene show equilibrium textural relations (see Section 2). The presence of garnet in equilibrium with titanite may indicate high-temperature metamorphic conditions (Wang et al., 2021). Garnet coronas on clinopyroxene and cpx-plag-qtz ± garnet paragenesis suggest re-equilibration after peak pressure and temperature. This inference is based on commonly observed clockwise P–T–t paths of pyroxene-garnet bearing granulites where coronal garnet grows during decompression at slightly higher, or almost equal, temperatures (e.g., Owen and Dostal, 1996). Recrystallised quartz is the largest mineral observed in thin-section; their large angle of contact suggests that they were annealed at high temperatures. Finally, the presence of scapolite (i.e. a high-temperature reaction product of plagioclase) confirms that this sample reached high-grade metamorphic conditions in granulite facies (Winkler, 1976). The similar REE patterns observed in layers with different SiO_2 contents could be the result of deformation at subsolidus conditions during shearing, which preferentially decompose tabular mafic minerals (amphibole and biotite) that have low competence compared to felsic minerals. Zircon U—Pb ages and petrological observations suggest that no magmatic event occurred after ~2.2 Ga, and that ~1.9 Ga ages are restricted to subsolidus recrystallisation during metamorphism (Taylor et al., 2016; Schaltegger et al., 1999). Moreover, the rounded shape of zircons is typical of high-grade metamorphic grains widely described in the literature (Rubatto, 2017; Schaltegger et al., 1999). The protolith of sample 831–2 is expected to have a sedimentary origin because i) the large spread of zircon analyses along the Concordia curve (Fig. 8a) is typical of a detrital origin, and all zircons ranging in age ~ 2.6–2.2 Ga are (sub)concordant; and ii) several tectono-metamorphic events would be required to account for total resetting of the U—Pb system and age distribution, but these are not supported by registered events in the Anabar shield. Given that metamorphic conditions did not reach eclogitic facies and that this Palaeoproterozoic spread is defined by zircon cores with variable CL texture, a mixed detrital source is the most plausible protolith for this sample. These sediments probably derive from a Palaeoproterozoic passive margin, given the large proportion of zircons with crystallisation ages older than the ~2.2 Ga maximum depositional age of the sediment (following the model of Cawood et al., 2012). The maximum depositional age is inferred from the age of the youngest concordant zircon core, dated at 2251 ± 15 Ma (analysis *#831–2_zr30c,* see Supplementary file). This passive margin sedimentary sequence may have been part of the Palaeoproterozoic belt from the Khapchan Group, which collided with the Archaean west portion of the shield at ~2.0 Ga (Gusev et al., 2021).

The composition and mineralogy of sample 601A suggest a sandstone as a likely protolith. Metamorphism is marked by the presence of a proto-mylonitic foliation, along with recrystallised quartz. Garnet growth preceded mylonitic deformation because garnet is aligned within the main foliation, and it shows corrosion features suggesting that partial breakdown occurred during deformation. Incipient acicular crystals of sillimanite in contact with garnet suggest that the sandstone experienced high-temperature conditions during garnet growth. The assemblage Kfspar-sillimanite indicates that any muscovite that may have been originally present was consumed (Winkler, 1976). Zircon cores show fine oscillatory zoning and lower luminescence compared to rim overgrowths (Fig. 8b). The age of the core population is unimodal, and the $^{207}Pb/^{206}Pb$ age peak at ~3.6 Ga with similar $^{176}Hf/^{177}Hf$ ratios is interpreted as the main detrital source of the sandstone protolith (Fig. 9). The lower intercept at ~1.9 Ga in the Concordia plot (Fig. 8b) coincides with zircon rims ages ca. 1945 ± 28 Ma. The remarkable absence of biotite or micas in thin-section suggest heating towards peak temperature, which produced sillimanite, garnet and K-feldspar after biotite. These high-grade metamorphic minerals define the main foliation, which suggests that they grew before mylonitization. Thus, mylonitization should have occurred at peak to slightly lower temperature to produce a fabric containing unretrogressed high grade minerals and annealed quartz. It is therefore suggested that zircon growth occurred during the high temperature metamorphism of this rock when garnet was stable.

5.1.2. Metaigneous rocks

Sample 607 is characterised by a distinct retrogression reaction from granulite to amphibolite facies (Fig. 5). Although zircon metamorphic reactions in granulites are not well documented (aside from baddeleyite + $SiO_2 = ZrSiO_4$; e.g., Davidson and Van Breemen, 1988), there is clear textural evidence for dissolution of older zircons (Fig. 8). Other reactions upon release of SiO_2 must involve the incorporation of Zr + Hf in trace amounts in mafic minerals, and perhaps also rutile. For example, the breakdown of pyroxene releases SiO_2, and the common reaction in mafic

granulites is opx + cpx + plag+H_2O + Ti-magnetite = Hbl + qtz + plag (Winkler, 1976). Since granulites that have not retrogressed to amphibolite facies are richer in magnetite (Fig. 5), and since amphibole can contain fair amounts of Ti (i.e. around 1.5%), the above reaction is a reasonable explanation for the paragenesis of sample 607. This reaction may be related to the dissolution of older grains and recrystallisation of zircon rims at ~1.9 Ga (Fig. 8c,d,e). Samples 607A and 607B have widespread recrystallised quartz, and the angle between recrystallised quartz and other phases is high (>120°), which suggests equilibration at high temperatures. The whole-rock REE and SiO_2 variation in samples 607, 607A and 607B likely represents primary heterogeneity within the mafic protolith (Fig. 7). The subtraction of mafic minerals (pyroxene /amphibole) upon melt segregation depletes REE from high SiO_2 melts at the same time it reduces the negative Eu anomaly as the modal proportion of feldspar increases (Pu et al., 2014; Laurent et al., 2020). It is also possible that the reaction that generated the high SiO_2 / REE-depleted sample has progressed to high degrees of melting, yielding to the extraction of more evolved melts with high SiO_2 but reduced REE contents (Brophy, 2008). Zircon age distributions are similar in the three samples from locality 607. Most of the U—Pb analyses in zircon cores project an upper intercept in the Concordia at ~3.3 Ga and have similar $^{176}Hf/^{177}Hf$ ratios (Figs. 8,9), thus 3.3 Ga may represent the age for the mafic protolith. Sub-concordant U—Pb analyses with different amounts of Pb-loss plot on a discordia line from the possible protolith age towards 2.0–1.9 Ga, which coincides with the rim ages and is interpreted as the metamorphic age. This ancient Pb-loss pattern is characteristic of granulite facies metamorphism (Taylor et al., 2016). Older zircon cores (> 3.3 Ga) are interpreted as inherited, with ages as old as 3.8 Ga.

Sample 177 shows important features of recrystallisation, such as high-angle quartz morphology, as well as stretching and obliteration of more ductile primary biotites (see Section 2). The protolith of this meta-granitoid likely derived from the melting of a lower mafic crust in the presence of garnet and absence of feldspar, as suggested by the relative depletion of overall REE and the absence of Eu anomaly. The upper intercept age in the Concordia diagram, calculated based on the 8 oldest and most concordant zircon cores with fine oscillatory CL zoning, similar $^{176}Hf/^{177}Hf$ (0.280610 ± 0.0001; 2 SD) and high Th/U ratios suggests a crystallisation age at 3359 ± 76 Ma (Fig. 8f). Zircon rim analyses are discordant, yet their $^{207}Pb/^{206}Pb$ ages are within error of the metamorphic age of 1926 ± 38 Ma previously calculated in concordant rim analyses for the same sample (Gusev 2017).

In summary, the Anabar shield samples contain zircons with core ages ranging from 3.8 to 2.2 Ga, surrounded by rims with a much narrower age range, from 2.0 to 1.9 Ga. In addition, some zircon grains look uniform, have structureless CL imaging and also range in age from 2.0 to 1.9 Ga (Fig. 8). Ages of zircon rims match the regional granulite facies event in the Anabar shield, initially dated at 1919 ± 13 Ma by Sm—Nd isochron (whole-rock + garnets) in a grt-opx-plg gneiss (Sergeeva et al., 2018).

5.2. High-grade metamorphism at subsolidus conditions

There is a considerable debate over the presence or absence of melt during zircon recrystallisation and growth (e.g., Hoskin and Black, 2000; Corfu, 2007; Harley and Kelly, 2007; Thakurdin et al., 2019). In this section we show that taking into account textural aspects and zoning features of zircon grains, in combination with detailed petrogenetic information on their host rocks, have the potential to move the debate forward.

The parageneses of Anabar samples are primarily anhydrous, with minor hydrous minerals either as re-equilibration phases at low metamorphic grades, or as products of retrogression reactions (Figs. 4, 5 and 6). In the mafic granulites from locality 607, biotite is scarce and only found as alteration products in sheared layers. Amphiboles mainly result from retrogression of pyroxene. In felsic granulite (sample 831–2), the presence of garnet and two pyroxenes (besides garnet coronas in augite) indicates medium and high-pressure conditions, with continuous reactions between garnet, clinopyroxene and plagioclase. Titanite and magnetite are common in the felsic granulites and the absence of rutile indicates either retrogression or that higher pressures were not reached (Kohn, 2017). Although direct pressure-temperature constraints are not available for our samples, the presence of garnet, pyroxene, plagioclase, quartz and scapolite (sample 831–2), as well as the presence of two pyroxenes in mafic granulites (locality 607), indicate that they reached granulite metamorphic conditions and equilibrated at ≥700 °C and 0.7–1.0 GPa. This is consistent with previous studies, which have suggested that the ~1.9 Ga metamorphic event reached 775 ± 35 °C and 0.75 ± 0.07 GPa (Sergeeva et al., 2018). More recent estimates by Apen et al. (2022), using a range of garnet-pyroxene granulites from kimberlite xenoliths in the Anabar lower crust, suggest P–T conditions of 700–900 °C and 1.3 ± 0.4 GPa. Finally, after the samples reached granulite conditions, they equilibrated at upper amphibolite conditions (Perchuk et al., 2021).

Zircon rims and homogeneous zircons that crystallised between 2.0 and 1.9 Ga have overall higher Th/U ratios (>0.5) than those of zircon cores with older ages (Th/U = 0.1–0.5) (Fig. 10a), and their $^{176}Lu/^{177}Hf$ ratios are overall lower (i.e. <0.0005, with most of which <0.0003) than the variably higher ratios of the cores (Fig. 10b). This suggests that zircon overgrowths are metamorphic (Moreira et al., 2023) and formed at high temperature (>700 °C) in the absence of melt (e.g., Kunz et al., 2018). The similar age for the zircon rims and the regional metamorphism, alongside the presence of a ubiquitous population of euhedral and semi-spheric zircons, virtually free of inclusions (Fig. 7), suggest that they have experienced high-grade metamorphism under dry conditions. High-grade metamorphic zircon domains are commonly free of inclusions and have high Th/U ratios because they form in low fluid activity environments. As a result, the probability for other mineral phases to be incorporated into the growing zircon zone is low, leading to the absence of inclusions. For similar reasons, the co-crystallisation of high-Th fluid-associated phases, such as monazite, is unlikely, and growing zircon incorporates preferentially Th over U (e.g. Yakymchuk et al., 2018). Although it remains difficult to determine whether granulite retrogression via hydration has led to zircon recrystallisation, it certainly indicates the presence of fluids, but not melts (Hoskin and Black, 2000). Therefore, we argue that the 2.0–1.9 Ga period in the Anabar shield was dominated by high-grade metamorphism that intensified zircon dissolution and recrystallisation at subsolidus conditions (e.g., Taylor et al., 2016).

5.3. Impact of high-grade metamorphism on the zircon record

Unlike the U–Th–Pb system, Lu—Hf isotopes in zircon are not prone to resetting during metamorphism (Kinny and Maas, 2003; Hawkesworth and Kemp, 2006). As a consequence, the integrated analysis of U—Pb and Lu—Hf isotopes in targeted zircon growth domains can indicate whether growth occurred through magmatic crystallisation, or through dissolution/recrystallisation of pre-existing zircon(s) (Gerdes and Zeh, 2009). If zircons grow during different periods of magmatic crystallisation of the same source, $^{176}Hf/^{177}Hf$ ratios will increase as U—Pb crystallisation ages become younger. This feature is commonly observed at intra-grain scale, where cores and rims with different U—Pb ages have different Hf isotope ratios (e.g., Laurent et al., 2019; Petersson et al., 2019; Shatsky et al., 2022). In contrast, if zircons grow through dissolution/recrystallisation of pre-existing zircon(s), a population of zircons with similar $^{176}Hf/^{177}Hf$ ratios but variable $^{207}Pb/^{206}Pb$ ages may be identified (Guitreau and Blichert-Toft, 2014; Claesson et al., 2015; Vervoort and Kemp, 2016), and the data define what is commonly referred to as a 'Pb-loss trend' on the $^{176}Hf/^{177}Hf$ versus $^{207}Pb/^{206}Pb$ age plot (Fig. 8).

A change in both crystallisation ages and $^{176}Hf/^{177}Hf$ ratios can also result from zircon recrystallisation if high-Lu/Hf phases break down (Zheng et al., 2004; Shatsky et al., 2016; Chen et al., 2010; Kemp et al.,

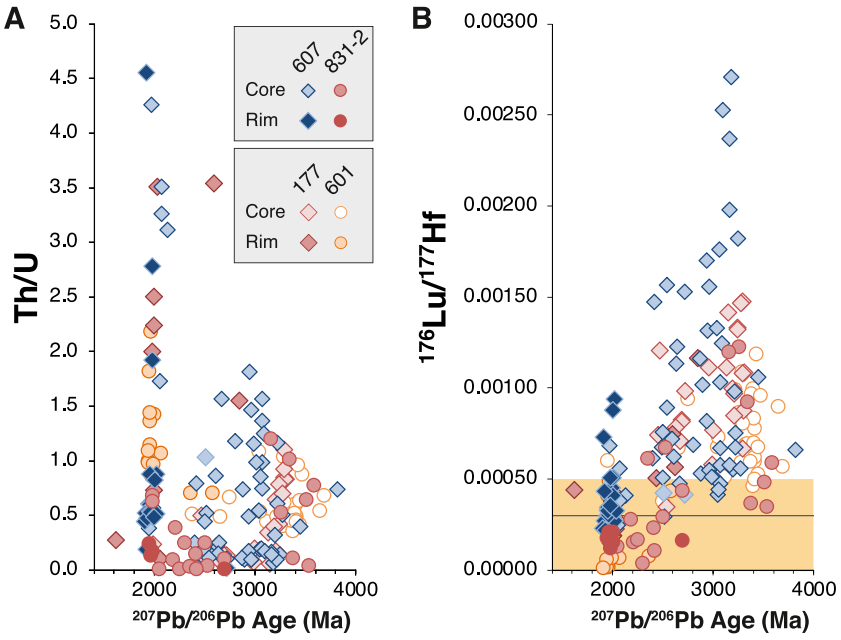

Fig. 10. Plot of Th/U and $^{176}Lu/^{177}Hf$ versus apparent $^{207}Pb/^{206}Pb$ ages. A) Th/U ratios are higher and more variable in zircon rims than in zircon cores. B) $^{176}Lu/^{177}Hf$ in zircon rims are lower than zircon cores and fall within the metamorphic classification field in orange. Black line indicates $^{176}Lu/^{177}Hf = 0.003$.

2019). Radiogenic Hf may build up in the high-Lu/Hf phases, and the amount of radiogenic Hf incorporated in these phases crucially depends on the time between their crystallisation and breakdown in a rock. If zircon recrystallises during the breakdown of high-Lu/Hf phases, Hf may be promptly incorporated by new zircon growth in the absence of melt. Although this phenomenon remains poorly documented in the literature, it can increase the $^{176}Hf/^{177}Hf$ ratios such that $\varepsilon Hf_{(t)}$ values increase by ~20 $\varepsilon Hf_{(t)}$ units (Zheng et al., 2004).

The $\varepsilon Hf_{(t)}$ variation as a function of the crystallisation age of Anabar shield zircons is summarised in Fig. 9, along with data from the literature. Assuming that the Lu—Hf system remains closed, and that the distribution of the data along evolution lines with $^{176}Lu/^{177}Hf = 0$ slopes is mainly caused by Pb-loss during zircon recrystallisation (black dashed arrows in Fig. 9), the timing of mantle-crust separation events can be reasonably estimated (e.g., Claesson et al., 2015). These events are represented by the red and yellow stars in Fig. 9, depending on whether new continental crust derived from a depleted mantle (red stars), or a chondritic mantle reservoir (yellow stars). Considering both reservoirs, it is reasonable to estimate major crustal formation events in the Siberian Craton at 2.7–3.0 Ga and 3.4–3.6 Ga. For comparison, the evolution of a typical crustal reservoir extracted from the depleted mantle at 3.95 Ga with $^{176}Lu/^{177}Hf = 0.015$ (green arrow; Fig. 9) shows that reworking is unlikely to account for the observed trends. The oldest zircon core dated in this study indicates a crust formation episode at 3.8 Ga from a chondritic source, or at ~4.1 Ga from a depleted mantle source. Although this observation only concerns a single grain, which could be exotic to the studied region, it argues for the presence of Eoarchaean remnants in the Siberian Craton.

A marked shift towards higher $\varepsilon Hf_{(t)}$ values occurs in the 2.0–1.8 Ga interval, where a large spread of subchondritic to superchondritic values is observed (Fig. 9). Overall, $\varepsilon Hf_{(t)}$ values at ~2.0–1.8 Ga define a vertical shift that is similar to those highlighted in Fig. 1. One classic interpretation for this upward shift is the addition of juvenile magmas during this time interval; however, this model is not consistent with the scarcity of ~2.0 Ga juvenile magmatic rocks in the centre of the Anabar shield. In general, ~2.0 Ga samples with superchondritic Hf isotopes are either attributed to tectonothermal events during craton formation (e.g., Moyen et al., 2017; Skuzovatov et al., 2022), or to scarce 2.06–2.00 Ga subduction-related granitoids more abundant in the southern Siberian Craton (Donskaya, 2020). Remarkably, the most positive $\varepsilon Hf_{(2000–1850\ Ma)}$ values in the literature come from zircon grains and recrystalised zircon rims around older cores in garnet-bearing granulites (Moyen et al., 2017; Shatsky et al., 2022; Skuzovatov et al., 2022). This suggests that intra-crustal differentiation and reactions between zircon and garnet were involved to produce high $^{176}Hf/^{177}Hf$ ratios.

The combination of Pb—Hf isotope evidence and petrological information indicates that subsolidus metamorphic reactions are the most likely explanation for the vertical shift between 2.0 and 1.8 Ga in the $\varepsilon Hf_{(t)}$-time array (Figs. 8 and 9). Perhaps surprisingly, samples 177 and 601A do not record an important $\varepsilon Hf_{(t)}$ variation at the peak of metamorphism (i.e. ~1.9 Ga). One possible explanation is that metamorphic zircons in these samples recrystallised in the absence of high-Lu/Hf phases in the matrix (Zheng et al., 2004). This implies that the minor amounts of garnet in sample 601A did not react out to release Hf during zircon recrystallisation (see Section 5.1). Alternatively, garnet may have formed at the metamorphic peak, which precludes production of large amounts of radiogenic Hf via Lu decay. It is also possible that zircons that did not incorporate extra radiogenic Hf recrystallised away from other Lu-rich phases (i.e. local control dependency). This would explain why most, but not all, recrystallised zircons from samples with abundant Lu-rich phases (831–2 and 607) show important Hf isotope variations.

Subsolidus metamorphic reactions may have no control over $^{176}Hf/^{177}Hf$ ratios in zircon if zircon crystallisation pre-dates garnet breakdown decompression reactions (Sláma et al., 2007). When high-Lu/Hf metamorphic minerals form and break down after or at the same time as zircon dissolves and recrystallises, there is not enough time for radiogenic Hf ingrowth and incorporation into newly recrystallised rims. This is not the case for the Anabar shield zircons in this work. Overall, this study indicates that radiogenic Hf variations in zircon can be caused by the breakdown of high-Lu/Hf phases, providing that the time between crystallisation and breakdown of the high-Lu/Hf phases was long enough to allow the accumulation of radiogenic Hf in their lattice.

5.4. Modelling the 'vertical shifts' in the $\varepsilon Hf_{(t)}$–age space

Shifts to higher $\varepsilon Hf_{(t)}$ values on $\varepsilon Hf_{(t)}$ vs. age plots are classically attributed to juvenile additions to the continental crust, with possible

links to global changes in the tectonic regime of crust generation (Bauer et al., 2020a, 2020b; Ranjan et al., 2020; Mulder et al., 2021; dos Santos et al., 2022; Drabon et al., 2022). Although a well-marked 'vertical shift' at 2.0–1.8 Ga is observed in the Anabar shield data, we found no evidence for additions of juvenile material at that time. Instead, we gathered compelling evidence for the input of radiogenic Hf released from the breakdown of high-Lu phases as zircon (re)crystallised. It remains unclear why the literature reported zircons with far more radiogenic Hf than the samples of this study (Fig. 11). Nonetheless, the petrologic evidence and comparisons with the literature data indicate that whilst garnet and pyroxene are present in Anabar samples 831–2 and 607, they are not as abundant as in lower crustal granulites sampled by kimberlite magmas (e.g., Moyen et al., 2017; Shatsky et al., 2022; Skuzovatov et al., 2022). Moreover, Anabar samples contain more Zr (~250 ppm) than lower crustal mafic granulite xenoliths (~100 ppm, Moyen et al., 2017), suggesting that Anabar samples have a greater proportion of inherited grains in their zircon population.

In Fig. 11 we developed a mixing model to explore radiogenic Hf incorporation during zircon recrystallisation in the presence of high-Lu/Hf phases and/or large amounts of inherited zircons. One major assumption of this model is that crustal extraction events should form high-Lu/Hf residues. The timing of these events was set at 3.5, 3.0 and 2.8 Ga, which correspond to major lithosphere formation events in the Anabar shield (Ionov et al., 2015; Doucet et al., 2015; Paquette et al., 2017). Garnet-pyroxene reservoirs are assumed to have formed as lower crust residues, with $^{176}Lu/^{177}Hf$ ratios of 0.0425, 0.0410 and 0.0500 at 3.5 Ga, 3.0 Ga and 2.8 Ga, respectively, based on the data of Doucet et al. (2015). The model shows that a garnet-pyroxene source can develop a high $^{176}Hf/^{177}Hf$ ratio if sufficient time is allowed for radiogenic ingrowth (green evolution lines). This observation is consistent with previous studies of high-Lu/Hf reservoirs (e.g., Patchett et al., 1982; Salters and White, 1998; Hamelin et al., 2013). At 1.9 Ga, which is taken as the mean age of high-grade metamorphism in the Anabar shield, the garnet-pyroxene reservoirs reached $\varepsilon Hf_{(t)} = +12$. This value constitutes the first endmember of the model. The second endmember is the lowest $\varepsilon Hf_{(t)}$ value at 1.9 Ga obtained in this study, i.e. $\varepsilon Hf_{(t)} = -35$, which we interpret as the time of dissolution of ancient protolith/inherited zircons. The metamorphic reaction at 1.9 Ga is modelled from the mixing between a 'high-Lu/Hf source' with $\varepsilon Hf_{(t)} = +12$ (50% of garnet and/or pyroxene with 5 ppm Hf), and a 'zircon source' with $\varepsilon Hf_{(t)} = -35$ (0.01% of zircon with 10,000 ppm Hf) (Fig. 9). The model shows that reactions involving 10 to 50% of radiogenic Hf from the 'high-Lu/Hf source endmember can increase the Hf isotope ratios of zircon during recrystallisation by >30 εHf units. Since $^{176}Lu/^{177}Hf$ ratios of garnet and/or pyroxene from Siberian mantle peridotites are high (>1; e.g., Doucet et al., 2015), the $\varepsilon Hf_{(t)}$ value of +12 at 1.9 Ga in our model must be considered as a lower estimate. This implies that shifts in the $\varepsilon Hf_{(t)}$-time array could be achieved with less garnet in the source protolith, and/or with more zircons available for dissolution/recrystallisation.

Our mixing model indicates that the overall effect of dissolution of ancient inherited zircons is to decrease the $^{176}Hf/^{177}Hf$ of new zircon overgrowths. However, the dissolution of inherited zircons may also produce variations in the opposite direction, that is towards higher $\varepsilon Hf_{(t)}$ values at 2.0–1.8 Ga at specific conditions. The $^{207}Pb/^{206}Pb$ ages of the major population of zircon cores range from 3.2 to 3.5 Ga (Fig. 7). These ancient zircons could experience variable degrees of dissolution and recrystallisation during the 1.9 Ga metamorphic event, which may reasonably explain their ancient Pb-loss trend on the Concordia diagram and the spread towards more negative $\varepsilon Hf_{(t)}$ values (Figs. 7, 8). If a complete Pb-loss of the 3.2 to 3.5 Ga cores occurred at 1.9 Ga, the zircons recrystallised at that time would have $\varepsilon Hf_{(t)}$ values between – 30 and – 40 (red background field; Fig. 9). This indicates that the total $^{176}Hf/^{177}Hf$ increase during dissolution and recrystallisation of zircons at ~1.9 Ga can only account for a maximum increase of ~10 εHf units. This is insufficient to explain the >45 εHf units variation observed in Fig. 11, and therefore, dissolution of inherited zircons is considered unlikely to produce large variation towards superchondritic $\varepsilon Hf_{(t)}$ values.

Another hypothesis for the increase of the $^{176}Hf/^{177}Hf$ ratios at ~1.9 Ga is the dissolution of zircons derived from a hypothetical highly radiogenic source at ~2.2 Ga, with for instance, $\varepsilon Hf_{(2200)} = +8$. At the time of dissolution, zircons would still have superchondritic εHf values (i.e. $\varepsilon Hf_{(1900)} = +4$), and may form a radiogenic endmember. We find this hypothesis unlikely because of the low overall abundance of zircons

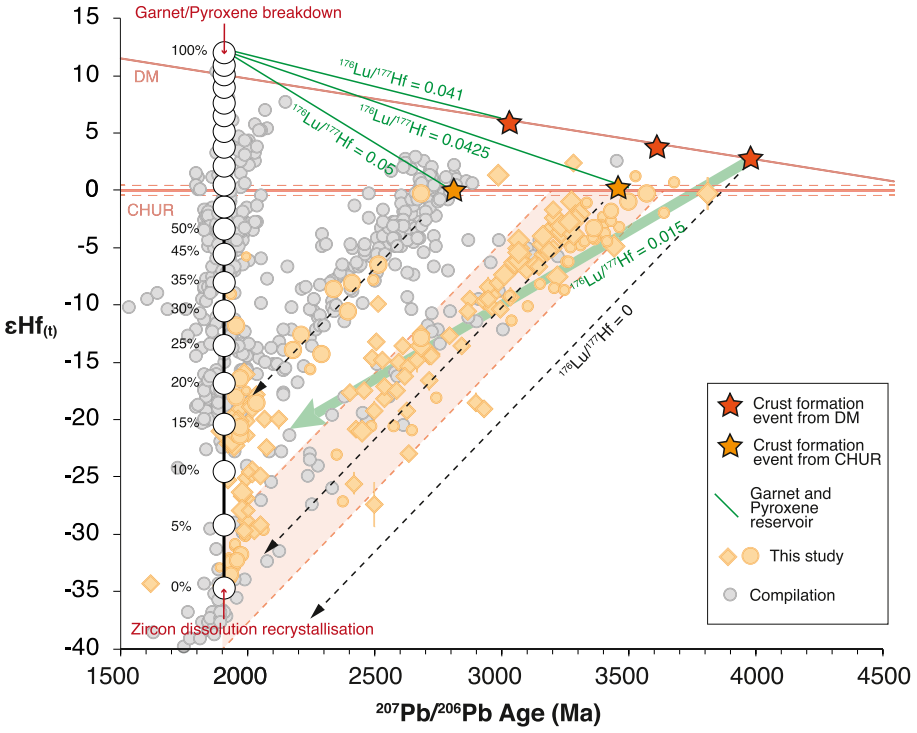

Fig. 11. Compilation of zircon isotope data for the Anabar shield (this study and literature data from Skuzovatov et al., 2022 and references therein). The model shows the percentage of high-Lu/Hf phases breakdown required to generate an increase in εHf at 1.9 Ga during zircon recrystallisation, from an initial lowest εHf value of −35. Garnet pyroxenites, which were previously formed as lower crust residues during the crust formation events represented by the orange and yellow stars, may have served as long-lived high-Lu/Hf reservoirs for radiogenic Hf ingrowth (dark green lines). Note that the high-Lu/Hf endmember at 1.9 Ga is a minimum estimate, as garnet-pyroxenites usually have higher $^{176}Lu/^{177}Hf$ than the indicated by the dark green lines. Black dashed arrows with $^{176}Lu/^{177}Hf$ slopes = 0 indicate Pb-loss trends, and the red background field highlights the isotope evolution of a large majority of zircon core analyses. The green arrow shows the evolution of a hypothetical 3.95 Ga crustal source with a $^{176}Lu/^{177}Hf$ ratio of 0.015. DM and CHUR evolution lines are after Chauvel and Blichert-Toft (2001) and Bouvier et al. (2008), respectively. (For interpretation of the references to colour in this figure legend, the reader is referred to the web version of this article.)

in the rocks of this study (i.e. < 0.05%), and because 2.4–2.0 Ga zircons with superchondritic values are not common in the Siberian Craton (Fig. 9). Moreover, the Lu/Hf ratios in garnet and pyroxene are usually two orders of magnitude higher than in zircon, and we posit that zircon dissolution plays a minor role in generating $\varepsilon Hf_{(t)}$ shifts to higher values (and conversely, a more important role in generating shifts towards lower values). Overall, the higher abundance of inherited zircons in the Anabar samples may therefore account for the less significant $\varepsilon Hf_{(t)}$ shifts towards higher values compared to those in the literature data.

5.5. An alternative geodynamic perspective for vertical shifts in the $\varepsilon Hf_{(t)}$–age space

The presence of vertical shifts in $\varepsilon Hf_{(t)}$ versus crystallisation age plots in Eoarchaean to Mesoarchaean zircons from southern West Greenland was initially used by Næraa et al. (2012) to evoke a major change in Earth's tectonic regime at ~3.2 Ga. More recently, a similar approach was used by Bauer et al. (2017) for Eoarchaean to Mesoarchaean samples from northern Canada (Acasta Gneiss Complex), with both elemental and isotope analyses suggesting a change in magma compositions from those produced by crustal reworking to predominantly juvenile at ~3.6 Ga (Amelin et al., 2000; Iizuka et al., 2009; Reimink et al., 2019). When combined to whole-rock La/Yb ratios as a proxy for crustal thickness, this change in magma generation was used to infer a transition from stagnant lid to mobile lid tectonics (Reimink et al., 2016; Bauer et al., 2020a, 2020b). This model was then extended to cratons worldwide using detrital zircon databases (e.g., Mulder et al., 2021; Drabon et al., 2022; dos Santos et al., 2022). While studies based on changes in the preserved geological record are compelling (e.g., Næraa et al., 2012; Bauer et al., 2017), the absence of geological context in detrital zircon studies makes interpretations more difficult to test. Our new data for the Anabar shield support an alternative model to produce vertical shifts in the $\varepsilon Hf_{(t)}$–age space, which does not involve the generation of juvenile crust and fundamental changes in tectonic settings.

Seismic data for the Siberian Craton show that the crustal thickness in the Anabar shield is ~50 km (Cherepanova et al., 2013), which is greater than the average value for the continental crust (35–40 km; Christensen and Mooney, 1995). Given the absence of orogeny-related events younger than ~2 Ga in the Anabar shield, the thickness of 50 km was likely reached during the ~2.0 Ga amalgamation/crustal thickening event (Rosen et al., 2006). Importantly, there is no evidence of voluminous magmatism during this event, and the latest magmatic activity is in the surrounding Palaeozoic and Mesozoic low-volume kimberlite fields (Moyen et al., 2017; Skuzovatov et al., 2022; Apen et al., 2022). Xenoliths brought to the surface by the kimberlite magmas indicate a high cratonic geotherm at the time of kimberlite eruption (i.e. at 300–400 Ma), with a ~ 230 km-thick lithosphere (Liu et al., 2022). They also indicate that the post-cratonisation aftermath was marked by a slow cooling as the lower crust remained at ~700 °C for the first 300 Myr (i.e., from 2.1 to 1.8 Ga) and then decreased quickly to ~300 °C until kimberlite eruption ages at 360 Ma (Apen et al., 2022).

Higher temperatures in the cratonic lithosphere at 2.1–1.8 Ga may be associated with the collision of the 2095–2030 Ma Palaeoproterozoic Khapchan magmatic arc (Gusev et al., 2021). The convergence and collision of the arc at the eastern side of the shield (Fig. 3) reached thermal peak at ~1970 Ma, matching the age of the collision between the Daldyn and Khapchan terranes (Smelov et al., 2012). The tectonic activity induced by the collision has presumably facilitated fluid circulation and mixing with supracrustal lithologies from various sources. This may have facilitated recrystallisation of zircons in the inner parts of the Anabar shield through thermal conduction from the hot arc, in a similar way as in other cratons worldwide (e.g., Aguilar et al., 2017). Our petrological data suggest that the interaction between sources and supracrustal rocks undergoing granulite facies metamorphism did not lead to partial melting, but allowed radiogenic Hf incorporation in recrystallising zircons. The subsequently relatively low geothermal gradients of cratonic lithosphere likely allowed the preservation of the continental crust, and thus of Palaeoproterozoic zircon grains.

The scale of early cratonization events in the Palaeoarchaean and Eoarchaean is unknown, but the generation and stabilisation of the continental lithosphere could stem from plume-induced events in the absence of mobile lid tectonics (e.g., Pearson et al., 2021; Xu et al., 2023). The thermal history of the central Siberian craton, particularly in the Palaeoproterozoic (Apen et al., 2022; Liu et al., 2022), suggest that earlier Archaean cratonization may have contributed to vertical shifts on plots of $\varepsilon Hf_{(t)}$ vs. crystallisation age (Fig. 1). We posit that hotter geotherms in the early Earth, associated with craton formation and subsequent rapid cooling, could (at least partly) explain the secular shift(s) in $\varepsilon Hf_{(t)}$ of the continental crust since its early formation.

Subsequent subaerial emergence and erosion of early cratons since the Mesoarchaean (Flament et al., 2008; Chowdhury et al., 2021; Wang et al., 2022) exhumed high-grade metamorphic rocks and discharged zircons into sedimentary basins. In the absence of any whole-rock textural control, metamorphic zircons with unusually high Th/U and overall round shape, such as those presented in this study, could be misinterpreted as detrital grains from magmatic sources. Metamorphic zircons with high Th/U ratios are generally observed in granulites and other high-temperature metamorphic rocks (Rubatto, 2017), and their relative proportion in the detrital zircon record has yet to be determined. Nonetheless, it is clear that they could have incorporated radiogenic Hf from the breakdown of high-Lu/Hf phases and, as such, be partially responsible for shifts on the Hf evolution plots. These findings call for considering alternative options when interpreting Hf isotope variations in the Hadean/Archaean and for novel proxies discriminating metamorphic and igneous zircons in the detrital record.

6. Conclusions

The Anabar shield offers a unique opportunity to study the secular evolution of the continental crust for over two billion years. We combine petrological and isotopic information from different rock types to better understand Hf isotope systematics in the context of high-grade metamorphism, and reach the following conclusions:

1) The zircon cores suggest that the crust on the Siberian Craton initially formed at 2.7–3.0 Ga and 3.4–3.6 Ga. A single zircon core crystallised at 3.8 Ga may represent the oldest lithospheric material preserved on the craton, although its exotic origin cannot be ruled out.
2) High-grade metamorphism is testified by subsolidus growth of zircon at granulite-facies conditions at around 1.9 Ga in the Anabar shield. This is consistent with previous studies and demonstrates that, with the exception of low-intensity 360 Ma kimberlite magmatism, the craton has remained thermally undisturbed since its formation at around 1.9 Ga.
3) Zircons from high-temperature granulites may have high Th/U ratios that differ from ratios commonly used in the literature for igneous-metamorphic discrimination. Inferences from detrital zircon studies that use such Th/U to exclude metamorphic grains could be biased by still including a fair proportion of metamorphic zircons.
4) A 'rejuvenation process', which is characterised by a pronounced upward vertical shift in the $\varepsilon Hf_{(t)}$-time array has been identified in the Anabar shield at 2.0–1.8 Ga,. This shift is observed in rocks with petrological evidence for breakdown of high-Lu/Hf phases (garnet and/or pyroxene). It cannot be caused by a fundamental change in magma generation, because zircon grains grew at subsolidus conditions.
5) Vertical shifts in the $\varepsilon Hf_{(t)}$ versus age space may not necessarily involve juvenile additions to the continental crust via arc-like flux melting or mobile lid tectonics. Instead, they could be formed during

high-grade metamorphism during breakdown of high-Lu/Hf phases (i.e. garnet and pyroxene) along with zircon dissolution and recrystallisation. High grade metamorphic events in the early Earth may be related to the generation of the first cratons in geodynamical settings that do not necessary require plate tectonics.

Declaration of Competing Interest

The authors declare that they have no known competing financial interests or personal relationships that could have appeared to influence the work reported in this paper.

Data availability

The data is available in the supplementary material.

Acknowledgments

This project was funded by the European Research Council under the European Union's Horizon 2020 research and innovation program (No 817934). We thank Christophe Nevado and Doriane Delmas for confectioning the thin-sections of this study and Frédéric Fernandez for assisting with CL zircon imaging. Tony Kemp and anonymous reviewer are thanked for constructive criticism. Marco Fiorentini is thanked for editorial handling.

Appendix A. Supplementary data

Supplementary data to this article can be found online at https://doi.org/10.1016/j.chemgeo.2023.121644.

References

Aguilar, C., Alkmim, F.F., Lana, C., Farina, F., 2017. Palaeoproterozoic assembly of the São Francisco craton, SE Brazil: new insights from U–Pb titanite and monazite dating. Precambrian Res. 289, 95–115.

Amelin, Y., Lee, D.C., Halliday, A.N., 2000. Early-middle Archaean crustal evolution deduced from Lu-Hf and U-Pb isotopic studies of single zircon grains. Geochim. Cosmochim. Acta 64 (24), 4205–4225.

Apen, F.E., Rudnick, R.L., Ionov, D.A., Cottle, J.M., Moyen, J.F., Golovin, A.V., Korsakov, A.V., 2022. Heat Transfer and Production in Cratonic Continental Crust: U-Pb Thermochronology of Xenoliths From the Siberian Craton. Geochem. Geophys. Geosys. 23 (10), e2022GC010497.

Armstrong, R.A., Compston, W., De Wit, M.J., Williams, I.S., 1990. The stratigraphy of the 3.5-3.2 Ga Barberton Greenstone Belt revisited: a single zircon ion microprobe study. Earth Planet. Sci. Lett. 101, 90–106.

Barrote, V.R., Nebel, O., Wainwright, A.N., Cawood, P.A., Hollis, S.P., Raveggi, M., 2022. Testing the advantages of simultaneous in-situ SmNd, Upb and elemental analysis of igneous monazite for petrochronological studies. An example from the late Archean, Penzance granite, Western Australia. Chem. Geol. 594, 120760.

Bauer, A.M., Fisher, C.M., Vervoort, J.D., Bowring, S.A., 2017. Coupled zircon Lu–Hf and U–Pb isotopic analyses of the oldest terrestrial crust, the> 4.03 Ga Acasta Gneiss Complex. Earth Planet. Sci. Lett. 458, 37–48.

Bauer, A.M., Reimink, J.R., Chacko, T., Foley, B.J., Shirey, S.B., Pearson, D.G., 2020a. Hafnium isotopes in zircons document the gradual onset of mobile-lid tectonics. Geochem. Perspect. Lett. 14, 1–6.

Bauer, A.M., Vervoort, J.D., Fisher, C.M., 2020b. Unraveling the complexity of zircons from the 4.0–2.9 Ga Acasta Gneiss complex. Geochim. Cosmochim. Acta 283, 85–102.

Belousova, E.A., Kostitsyn, Y.A., Griffin, W.L., Begg, G.C., O'reilly, Pearson, N.J., 2010. The growth of the continental crust: constraints from zircon Hf-isotope data. Lithos 119 (3–4), 457–466.

Blichert-Toft, J., Albarède, F., 1997. The Lu-Hf isotope geochemistry of chondrites and the evolution of the mantle-crust system. Earth Planet. Sci. Lett. 148 (1–2), 243–258.

Bouvier, A., Vervoort, J.D., Patchett, P.J., 2008. The Lu–Hf and Sm–Nd isotopic composition of CHUR: constraints from unequilibrated chondrites and implications for the bulk composition of terrestrial planets. Earth Planet. Sci. Lett. 273 (1–2), 48–57.

Brophy, J.G., 2008. A study of rare earth element (REE)–SiO_2 variations in felsic liquids generated by basalt fractionation and amphibolite melting: a potential test for discriminating between the two different processes. Contrib. Mineral. Petrol. 156, 337–357. https://doi.org/10.1007/s00410-008-0289-x.

Buzenchi, A., Moreira, H., Bruguier, O., Dhuime, B., Pritam, N., 2022. Evidence for Protracted Intracrustal Reworking of Palaeoarchaean Crust in the Pilbara Craton (Mount Edgar Dome, Western Australia). Lithosphere 2022 (Special 8).

Carignan, J., Hild, P., Mevelle, G., Morel, J., Yeghicheyan, D., 2001. Routine analyses of trace elements in geological samples using flow injection and low pressure on-line liquid chromatography coupled to ICP-MS: a study of geochemical reference materials BR, DR-N, UB-N, AN-G and GH. Geostand. Newslett. 25 (2–3), 187–198.

Cawood, P.A., Hawkesworth, C.J., Dhuime, B., 2012. Detrital zircon record and tectonic setting. Geology 40 (10), 875–878.

Chauvel, C., Blichert-Toft, J., 2001. A hafnium isotope and trace element perspective on melting of the depleted mantle. Earth Planet. Sci. Lett. 190 (3–4), 137–151.

Chen, R.X., Zheng, Y.F., Xie, L., 2010. Metamorphic growth and recrystallization of zircon: distinction by simultaneous in-situ analyses of trace elements, U–Th–Pb and Lu–Hf isotopes in zircons from eclogite-facies rocks in the Sulu orogen. Lithos 114 (1–2), 132–154.

Cherepanova, Y., Artemieva, I.M., Thybo, H., Chemia, Z., 2013. Crustal structure of the Siberian craton and the West Siberian basin: an appraisal of existing seismic data. Tectonophysics 609, 154–183.

Chowdhury, P., Mulder, J.A., Cawood, P.A., Bhattacharjee, S., Roy, S., Wainwright, A.N., Nebel, O., Mukherjee, S., 2021. Magmatic thickening of crust in non–plate tectonic settings initiated the subaerial rise of Earth's first continents 3.3 to 3.2 billion years ago. Proc. Natl. Acad. Sci. 118 (46), e2105746118.

Christensen, N.I., Mooney, W.D., 1995. Seismic velocity structure and composition of the continental crust: a global view. J. Geophys. Res. Solid Earth 100 (B6), 9761–9788.

Chu, N.C., Taylor, R.N., Chavagnac, V., Nesbitt, R.W., Boella, R.M., Milton, J.A., German, C.R., Bayon, G., Burton, K., 2002. Hf isotope ratio analysis using multi-collector inductively coupled plasma mass spectrometry: an evaluation of isobaric interference corrections. J. Anal. Atomic Spectrom. 17 (12), 1567–1574.

Claesson, S., Bibikova, E., Shumlyanskyy, L., Dhuime, B., Hawkesworth, C.J., 2015. The oldest crust in the Ukrainian Shield–Eoarchaean U–Pb ages and Hf–Nd constraints from enderbites and metasediments. Geol. Soc. Lond., Spec. Publ. 389 (1), 227–259.

Condie, K.C. (Ed.), 1994. Archean Crustal Evolution. Elsevier.

Corfu, F., 2007. Multistage metamorphic evolution and nature of the amphibolite–granulite facies transition in Lofoten–Vesterålen, Norway, revealed by U–Pb in accessory minerals. Chem. Geol. 241 (1–2), 108–128.

Davidson, A., Van Breemen, O., 1988. Baddeleyite-zircon relationships in coronitic metagabbro, Grenville Province, Ontario: implications for geochronology. Contrib. Mineral. Petrol. 100 (3), 291–299.

DePaolo, D.J., Wasserburg, G.J., 1976. Nd isotopic variations and petrogenetic models. Geophys. Res. Lett. 3 (5), 249–252.

Dhuime, B., Hawkesworth, C.J., Cawood, P.A., Storey, C.D., 2012. A change in the geodynamics of continental growth 3 billion years ago. Science 335 (6074), 1334–1336.

Donskaya, T.V., 2020. Assembly of the Siberian Craton: constraints from Paleoproterozoic granitoids. Precambrian Res. 348, 105869.

dos Santos, C., Zincone, S.A., Queiroga, G.N., Bersan, S.M., Lana, C.C., Oliveira, E.P., 2022. Evidence for change in crust formation process during the Paleoarchean in the São Francisco Craton (Gavião Block): coupled zircon Lu-Hf and U-Pb isotopic analyses and tectonic implications. Precambrian Res. 368, 106472.

Doucet, L.S., Ionov, D.A., Golovin, A.V., 2015. Paleoproterozoic formation age for the Siberian cratonic mantle: Hf and Nd isotope data on refractory peridotite xenoliths from the Udachnaya kimberlite. Chem. Geol. 391, 42–55.

Drabon, N., Byerly, B.L., Byerly, G.R., Wooden, J.L., Wiedenbeck, M., Valley, J.W., Kitajima, K., Bauer, A.M., Lowe, D.R., 2022. Destabilization of long-lived hadean Protocrust and the onset of pervasive hydrous melting at 3.8 Ga. AGU. Advances 3 (2) p.e2021AV000520.

Fisher, C.M., Bauer, A.M., Luo, Y., Sarkar, C., Hanchar, J.M., Vervoort, J.D., Tapster, S.R., Horstwood, M., Pearson, D.G., 2020. Laser ablation split-stream analysis of the Sm-Nd and U-Pb isotope compositions of monazite, titanite, and apatite–Improvements, potential reference materials, and application to the Archean Saglek Block gneisses. Chem. Geol. 539, 119493.

Fisher, C.M., Hanchar, J.M., Samson, S.D., Dhuime, B., Blichert-Toft, J., Vervoort, J.D., Lam, R., 2011. Synthetic zircon doped with hafnium and rare earth elements: A reference material for in situ hafnium isotope analysis. Chem. Geol. 286 (1–2), 32–47.

Fisher, C.M., Vervoort, J.D., 2018. Using the magmatic record to constrain the growth of continental crust—The Eoarchean zircon Hf record of Greenland. Earth Planet. Sci. Lett. 488, 79–91.

Flament, N., Coltice, N., Rey, P.F., 2008. A case for late-Archaean continental emergence from thermal evolution models and hypsometry. Earth Planet. Sci. Lett. 275 (3–4), 326–336.

Gerdes, A., Zeh, A., 2009. Zircon formation versus zircon alteration—new insights from combined U–Pb and Lu–Hf in-situ LA-ICP-MS analyses, and consequences for the interpretation of Archean zircon from the Central Zone of the Limpopo Belt. Chem. Geol. 261 (3–4), 230–243.

Guitreau, M., Blichert-Toft, J., 2014. Implications of discordant U–Pb ages on Hf isotope studies of detrital zircons. Chem. Geol. 385, 17–25.

Gusev, N.I., Sergeeva, L.Y., Skublov, S.G., Berezhnaya, N.G., Larionov, A.N., 2017. Composition and relations of Early and Late Archean granulites in the Bekelekh sequence of the Anabar shield (Siberian craton). Regionalnaya Geologiya i Metallogeniya 70, 17–35.

Gusev, N.I., Sergeeva, L.Y., Larionov, A.N., Skublov, S.G., 2020a. Relics of the Eoarchean continental crust of the Anabar Shield, Siberian Craton. Petrology 28 (2), 118–140.

Gusev, N.I., Sergeeva, L.Y., Skublov, S.G., 2020b. Dating the sedimentary protolith of the Daldyn Group Quartzite, Anabar Shield, Russia: new detrital zircon constraints. Geosciences 10 (6), 208.

Gusev, N.I., Sergeeva, L.Y., Skublov, S.G., 2021. Evidence of Subduction of the Paleoproterozoic Oceanic Crust in the Khapchan Belt of the Anabar Shield, Siberian Craton. Petrology 29 (2), 95–113.

Hamelin, C., Bezos, A., Dosso, L., Escartin, J., Cannat, M., Mevel, C., 2013. Atypically depleted upper mantle component revealed by Hf isotopes at Lucky strike segment. Chem. Geol. 341, 128–139.
Hammerli, J., Kemp, A.I., 2021. Combined Hf and Nd isotope microanalysis of co-existing zircon and REE-rich accessory minerals: High resolution insights into crustal processes. Chem. Geol. 581, 120393.
Harley, S.L., Kelly, N.M., 2007. The impact of zircon–garnet REE distribution data on the interpretation of zircon U–Pb ages in complex high-grade terrains: an example from the Rauer Islands, East Antarctica. Chem. Geol. 241 (1–2), 62–87.
Hawkesworth, C.J., Kemp, A.I.S., 2006. Using hafnium and oxygen isotopes in zircons to unravel the record of crustal evolution. Chem. Geol. 226 (3–4), 144–162.
Hoskin, P.W.O., Black, L.P., 2000. Metamorphic zircon formation by solid-state recrystallization of protolith igneous zircon. J. Metamorph. Geol. 18 (4), 423–439.
Iizuka, T., Komiya, T., Johnson, S.P., Kon, Y., Maruyama, S., Hirata, T., 2009. Reworking of Hadean crust in the Acasta gneisses, northwestern Canada: evidence from in-situ Lu–Hf isotope analysis of zircon. Chem. Geol. 259 (3–4), 230–239.
Ionov, D.A., Doucet, L.S., Carlson, R.W., Golovin, A.V., Korsakov, A.V., 2015. Post-Archean formation of the lithospheric mantle in the central Siberian craton: Re–Os and PGE study of peridotite xenoliths from the Udachnaya kimberlite. Geochim. Cosmochim. Acta 165, 466–483.
Ionov, D.A., Liu, Z., Li, J., Golovin, A.V., Korsakov, A.V., Xu, Y., 2020. The age and origin of cratonic lithospheric mantle: Archean dunites vs. Paleoproterozoic harzburgites from the Udachnaya kimberlite, Siberian craton. Geochimica et Cosmochimica Acta 281, 67–90.
Kemp, A.I., Whitehouse, M.J., Vervoort, J.D., 2019. Deciphering the zircon Hf isotope systematics of Eoarchean gneisses from Greenland: implications for ancient crust-mantle differentiation and Pb isotope controversies. Geochim. Cosmochim. Acta 250, 76–97.
Kemp, A.I.S., Wilde, S.A., Hawkesworth, C.J., Coath, C.D., Nemchin, A., Pidgeon, R.T., Vervoort, J.D., DuFrane, S.A., 2010. Hadean crustal evolution revisited: new constraints from Pb–Hf isotope systematics of the Jack Hills zircons. Earth Planet. Sci. Lett. 296 (1–2), 45–56.
Kinny, P.D., Maas, R., 2003. Lu–Hf and Sm–Nd isotope systems in zircon. Rev. Mineral. Geochem. 53 (1), 327–341.
Kirkland, C.L., Hartnady, M.I.H., Barham, M., Olierook, H.K.H., Steenfelt, A., Hollis, J.A., 2021. Widespread reworking of Hadean-to-Eoarchean continents during Earth's thermal peak. Nat. Commun. 12 (1), 331.
Kohn, M.J., 2017. Titanite petrochronology. Rev. Mineral. Geochem. 83 (1), 419–441.
Koreshkova, M., Downes, H., 2021. The age of the lower crust of the central part of the Columbia supercontinent: a review of zircon data. Gondwana Res. 96, 37–55.
Koreshkova, M.Y., Downes, H., Levsky, L.K., Vladykin, N.V., 2011. Petrology and geochemistry of granulite xenoliths from Udachnaya and Komsomolskaya kimberlite pipes, Siberia. J. Petrol. 52 (10), 1857–1885.
Kostrovitsky, S.I., Skuzovatov, S.Y., Yakovlev, D.A., Sun, J., Nasdala, L., Wu, F.-Y., 2016. Age of the Siberian craton crust beneath the northern kimberlite fields: insights to the craton evolution. Gondwana Res. 39, 365–385.
Kunz, B.E., Regis, D., Engi, M., 2018. Zircon ages in granulite facies rocks: decoupling from geochemistry above 850° C? Contrib. Mineral. Petrol. 173, 1–21.
Laurent, O., Martin, H., Moyen, J.F., Doucelance, R., 2014. The diversity and evolution of late-Archean granitoids: evidence for the onset of "modern-style" plate tectonics between 3.0 and 2.5 Ga. Lithos 205, 208–235.
Laurent, O., Björnsen, J., Wotzlaw, J.F., Bretscher, S., Pimenta Silva, M., Moyen, J.F., Ulmer, P., Bachmann, O., 2020. Earth's earliest granitoids are crystal-rich magma reservoirs tapped by silicic eruptions. Nat. Geosci. 13 (2), 163–169.
Laurent, O., Vander Auwera, J., Bingen, B., Bolle, O., Gerdes, A., 2019. Building up the first continents: Mesoarchean to Paleoproterozoic crustal evolution in West Troms, Norway, inferred from granitoid petrology, geochemistry and zircon U-Pb/Lu-Hf isotopes. Precambrian Res. 321, 303–327.
Liu, Z., Ionov, D.A., Nimis, P., Xu, Y., He, P., Golovin, A.V., 2022. Thermal and compositional anomalies in a detailed xenolith-based lithospheric mantle profile of the Siberian craton and the origin of seismic midlithosphere discontinuities. Geology 50 (8), 891–896.
Moreira, H., Buzenchi, A., Hawkesworth, C.J., Dhuime, B., 2023. Plumbing the depths of magma crystallization using 176Lu/177Hf in zircon as a pressure proxy. Geology 51 (3), 233–237.
Moyen, J.F., 2020. Archean granitoids: classification, petrology, geochemistry and origin. Geol. Soc. Lond., Spec. Publ. 489 (1), 15–49.
Moyen, J.F., Martin, H., 2012. Forty years of TTG research. Lithos 148, 312–336.
Moyen, J.F., Paquette, J.L., Ionov, D.A., Gannoun, A., Korsakov, A.V., Golovin, A.V., Moine, B.N., 2017. Paleoproterozoic rejuvenation and replacement of Archaean lithosphere: evidence from zircon U–Pb dating and Hf isotopes in crustal xenoliths at Udachnaya, Siberian craton. Earth Planet. Sci. Lett. 457, 149–159.
Mulder, J.A., Nebel, O., Gardiner, N.J., Cawood, P.A., Wainwright, A.N., Ivanic, T.J., 2021. Crustal rejuvenation stabilised Earth's first cratons. Nat. Commun. 12 (1), 3535.
Næraa, T., Scherstén, A., Rosing, M.T., Kemp, A.I.S., Hoffmann, J.E., Kokfelt, T.F., Whitehouse, M.J., 2012. Hafnium isotope evidence for a transition in the dynamics of continental growth 3.2 Gyr ago. Nature 485 (7400), 627–630.
Neymark, L.A., Nemchin, A.A., Rozen, O.M., Serenko, V.P., Spetsius, Z.V., Shuleshko, I. K., 1993. Sm-Nd Isotpe systems in lower-crust xenoliths from kimberlites of yakutia. Trans. USSR Acad. Sci. Earth Sci. Sect. 329 (3), 88–93.
Owen, J.V., Dostal, J., 1996. Contrasting corona structures in mafic granulite from the Blansky Les complex, Bohemian Massif, Czech Republic. Can. Mineral. 34 (5), 959–966.
Paquette, J.L., Ionov, D.A., Agashev, A.M., Gannoun, A., Nikolenko, E.I., 2017. Age, provenance and Precambrian evolution of the Anabar shield from U-Pb and Lu-Hf isotope data on detrital zircons, and the history of the northern and central Siberian craton. Precambrian Res. 301, 134–144.
Patchett, P., Kouvo, O., Hedge, C.E., Tatsumoto, M., 1982. Evolution of continental crust and mantle heterogeneity: evidence from Hf isotopes. Contrib. Mineral. Petrol. 78 (3), 279–297.
Patchett, P.J., Tatsumoto, M., 1981. A routine high-precision method for Lu-Hf isotope geochemistry and chronology. Contrib. Mineral. Petrol. 75, 263–267.
Paton, C., Hellstrom, J., Paul, B., Woodhead, J., Hergt, J., 2011. Iolite: Freeware for the visualisation and processing of mass spectrometric data. J. Anal. At. Spectrom. 26 (12), 2508–2518.
Pearson, D.G., Scott, J.M., Liu, J., Schaeffer, A., Wang, L.H., van Hunen, J., Szilas, K., Chacko, T., Kelemen, P.B., 2021. Deep continental roots and cratons. Nature 596 (7871), 199–210.
Perchuk, A.L., Sapegina, A.V., Safonov, O.G., Yapaskurt, V.O., Shatsky, V.S., Malkovets, V.G., 2021. Reduced amphibolite facies conditions in the Precambrian continental crust of the Siberian craton recorded by mafic granulite xenoliths from the Udachnaya kimberlite pipe, Yakutia. Precambrian Res. 357, 106122.
Petersson, A., Kemp, A.I., Whitehouse, M.J., 2019. A Yilgarn seed to the Pilbara Craton (Australia)? Evidence from inherited zircons. Geology 47 (11), 1098–1102.
Petrus, J.A., Kamber, B.S., 2012. VizualAge: A novel approach to laser ablation ICP-MS U-Pb geochronology data reduction. Geostand. Geoanal. Res. 36 (3), 247–270.
Priyatkina, N., Khudoley, A.K., Collins, W.J., Kuznetsov, N.B., Huang, H.-Q., 2016. Detrital zircon record of Meso- and Neoproterozoic sedimentary basins in northern part of the Siberian Craton: Characterizing buried crust of the basement. Precambrian Res. 285, 21–38.
Pu, X., Brophy, J.G., Tsujimori, T., 2014. Rare earth element–SiO_2 systematics of island arc crustal amphibolite migmatites from the Asago body of the Yakuno Ophiolite, Japan: a field evaluation of some model predictions. Contrib. Mineral. Petrol. 168, 1060. https://doi.org/10.1007/s00410-014-1060-0.
Puetz, S.J., Condie, K.C., 2019. Time series analysis of mantle cycles part I: periodicities and correlations among seven global isotopic databases. Geosci. Front. 10 (4), 1305–1326.
Ranjan, S., Upadhyay, D., Pruseth, K.L., Nanda, J.K., 2020. Detrital zircon evidence for change in geodynamic regime of continental crust formation 3.7–3.6 billion years ago. Earth Planet. Sci. Lett. 538, 116206.
Reimink, J.R., Chacko, T., Stern, R.A., Heaman, L.M., 2016. The birth of a cratonic nucleus: lithogeochemical evolution of the 4.02–2.94 Ga Acasta Gneiss complex. Precambrian Res. 281, 453–472.
Reimink, J.R., Pearson, D.G., Shirey, S.B., Carlson, R.W., Ketchum, J.W.F., 2019. Onset of new, progressive crustal growth in the central Slave craton at 3.55 Ga. Geochem. Perspect. Lett 10, 8–13.
Roberts, N.M., Spencer, C.J., 2015. The Zircon Archive of Continent Formation through Time. The Geological Society of London, London.
Rosen, O.M., Turkina, O.M., 2007. The oldest rock assemblages of the Siberian craton. In: Developments in Precambrian geology, 15, pp. 793–838.
Rosen, O.M., Condie, K.C., Natapov, L.M., Nozhkin, A.D., 1994. Archean and early Proterozoic evolution of the Siberian craton: A preliminary assessment. In: Developments in Precambrian Geology, vol. 11. Elsevier, pp. 411–459.
Rosen, O.M., Levskii, L.K., Zhuravlev, D.Z., Rotman, A.Y., Spetsius, Z.V., Makeev, A.F., Zinchuk, N.N., Manakov, A.V., Serenko, V.P., 2006. Paleoproterozoic accretion in the Northeast Siberian craton: Isotopic dating of the Anabar collision system. Stratigr. Geol. Correl. 14 (6), 581–601.
Rubatto, D., 2017. Zircon: the metamorphic mineral. Rev. Mineral. Geochem. 83 (1), 261–295.
Salters, V.J., White, W.M., 1998. Hf isotope constraints on mantle evolution. Chem. Geol. 145 (3–4), 447–460.
Schaltegger, U., Fanning, C.M., Günther, D., Maurin, J.C., Schulmann, K., Gebauer, D., 1999. Growth, annealing and recrystallization of zircon and preservation of monazite in high-grade metamorphism: conventional and in-situ U-Pb isotope, cathodoluminescence and microchemical evidence. Contrib. Mineral. Petrol. 134 (2), 186–201.
Sergeeva, L.Y., Berezin, A.V., Gusev, N.I., Skublov, S.G., Melnik, A.E., 2018. Age and metamorphic conditions of the granulites from Capral-Jegessky Synclinoria, Anabar Shield. Записки Горного института 229, 13–21.
Shatsky, V.S., Malkovets, V.G., Belousova, E.A., Tretiakova, I.G., Griffin, W.L., Ragozin, A.L., Gibsher, A.A., O'Reilly, S.Y., 2016. Tectonothermal evolution of the continental crust beneath the Yakutian diamondiferous province (Siberian craton): U–Pb and Hf isotopic evidence on zircons from crustal xenoliths of kimberlite pipes. Precambrian Res. 282, 1–20.
Shatsky, V.S., Wang, Q., Skuzovatov, S.Y., Ragozin, A.L., 2019. The crust-mantle evolution of the Anabar tectonic province in the Siberian Craton: coupled or decoupled? Precambrian Res. 332, 105388.
Shatsky, V.S., Ragozin, A.L., Wang, Q., Wu, M., 2022. Evidence of Eoarchean crust beneath the Yakutian kimberlite province in the Siberian craton. Precambrian Res. 369, 106512.
Skuzovatov, S.Y., Shatsky, V.S., Wang, Q., Ragozin, A.L., Kostrovitsky, S.I., 2022. Multiple tectonomagmatic reactivation of the unexposed basement in the northern Siberian craton: from Paleoproterozoic orogeny to Phanerozoic kimberlite magmatism. Int. Geol. Rev. 64 (8), 1119–1138.
Sláma, J., Košler, J., Pedersen, R.B., 2007. Behaviour of zircon in high-grade metamorphic rocks: evidence from Hf isotopes, trace elements and textural studies. Contrib. Mineral. Petrol. 154 (3), 335–356.
Sláma, J., Košler, J., Condon, D.J., Crowley, J.L., Gerdes, A., Hanchar, J.M., Horstwood, M.S., Morris, G.A., Nasdala, L., Norberg, N., Schaltegger, U., 2008. Plešovice zircon—a new natural reference material for U–Pb and Hf isotopic microanalysis. Chem. Geol. 249 (1–2), 1–35.

Smelov, A.P., Kotov, A.B., Sal'nikova, E.B., Kovach, V.P., Beryozkin, V.I., Kravchenko, A. A., Dobretsov, V.N., Velikoslavinskii, S.D., Yakovleva, S.Z., 2012. Age and duration of the formation of the Billyakh tectonic melange zone, Anabar Shield. Petrology 20 (3), 286–300.

Smith, P.E., Tatsumoto, M., Farquhar, R.M., 1987. Zircon Lu-Hf systematics and the evolution of the Archean crust in the southern Superior Province, Canada. Contrib. Mineral. Petrol. 97 (1), 93–104.

Taylor, R.J., Kirkland, C.L., Clark, C., 2016. Accessories after the facts: Constraining the timing, duration and conditions of high-temperature metamorphic processes. Lithos 264, 239–257.

Thakurdin, Y., Bolhar, R., Horváth, P., Wiedenbeck, M., Rocholl, A., 2019. Formation of lower to middle crust of the Wyoming Craton, Montana (USA), using evidence from zircon Hf-O isotopic and trace element compositions. Chem. Geol. 525, 218–244.

Vervoort, J.D., Kemp, A.I., 2016. Clarifying the zircon Hf isotope record of crust–mantle evolution. Chem. Geol. 425, 65–75.

Wang, J.M., Lanari, P., Wu, F.Y., Zhang, J.J., Khanal, G.P., Yang, L., 2021. First evidence of eclogites overprinted by ultrahigh temperature metamorphism in Everest East, Himalaya: Implications for collisional tectonics on early Earth. Earth Planet. Sci. Lett. 558, 116760.

Vervoort, J.D., Patchett, P.J., Söderlund, U., Baker, M., 2004. Isotopic composition of Yb and the determination of Lu concentrations and Lu/Hf ratios by isotope dilution using MC-ICPMS. Geochem. Geophys. Geosys. 5 (11).

Wang, W., Cawood, P.A., Spencer, C.J., Pandit, M.K., Zhao, J.H., Xia, X.P., Zheng, J.P., Lu, G.M., 2022. Global-scale emergence of continental crust during the Mesoarchean–early Neoarchean. Geology 50 (2), 184–188.

Whitehouse, M.J., Kemp, A.I., Petersson, A., 2022. Persistent mildly supra-chondritic initial Hf in the Lewisian complex, NW Scotland: implications for Neoarchean crust-mantle differentiation. Chem. Geol. 606, 121001.

Wiedenbeck, M.A.P.C., Alle, P., Corfu, F.Y., Griffin, W.L., Meier, M., Oberli, F.V., Quadt, A.V., Roddick, J.C., Spiegel, W., 1995. Three natural zircon standards for U-Th-Pb, Lu-Hf, trace element and REE analyses. Geostand. Newslett. 19 (1), 1–23.

Winkler, Helmut G.F., 1976. Petrogenesis of Metamorphic Rocks. Springer, New York. https://doi.org/10.1007/978-1-4757-4215-2, 1976 - Juvenile Nonfiction - 334 pages.

Woodhead, J.D., Hergt, J.M., 2005. A preliminary appraisal of seven natural zircon reference materials for in situ Hf isotope determination. Geostand. Geoanal. Res. 29 (2), 183–195.

Xu, X., Chen, H., Zuza, A.V., Yin, A., Yu, P., Lin, X., Zhao, C., Luo, J., Yang, S., Wang, B., 2023. Phanerozoic cratonization by plume welding. Geology. https://doi.org/10.1130/G50615.1 in press.

Yakymchuk, C., Kirkland, C.L., Clark, C., 2018. Th/U ratios in metamorphic zircon. J. Metamorph. Geol. 36 (6), 715–737.

Zheng, J., Griffin, W.L., O'Reilly, S.Y., Lu, F., Yu, C., Zhang, M., Li, H., 2004. U–Pb and Hf-isotope analysis of zircons in mafic xenoliths from Fuxian kimberlites: evolution of the lower crust beneath the North China Craton. Contrib. Mineral. Petrol. 148 (1), 79–103.